Russian Chemical Reviews **81** (1) 44 – 64 (2012) © 2012 Russian Academy of Sciences and Turpion Ltd

DOI 10.1070/RC2012v081n01ABEH004209

Accelerated mass transfer involving the liquid phase in solids

V V Belousov, S V Fedorov

Contents

I.	Introduction	44
II.	Thermodynamics of grain-boundary wetting in polycrystalline materials	45
III.	The liquid-channel grain-boundary structures	53
IV.	Accelerated mass transfer in ion-transport membranes and oxide layers	54

Abstract. The results of theoretical and experimental research on accelerated mass transfer involving the liquid phase in solids are analyzed. The kinetic regularities of mass transfer, the thermodynamics of grain-boundary wetting and the mechanisms of formation of liquid-channel grain boundary structure in polycrystalline materials are considered. The possibility of design of new membrane materials based on solid oxide – oxide melt composites and possessing high mixed ionic-electronic conductivity is demonstrated. The bibliography includes 224 references.

I. Introduction

The foundations of the classical theory of mass transfer in solids were laid by Frenkel, Schottky and Wagner in the 1930s. This theory is based on the concept of structural disorder. Most solid-state reactions involve mass and charge transfer; consequently, structural disorder is a key factor determining the reactivity of solids. In recent decades, ionic materials with high degree of structural disorder and, therefore, high ionic conductivity were created on the basis of stabilized zirconia, ceria, bismuth oxide, as well as copper and silver chalcogenides, a family of BIMEVOX solid solutions, perovskites, *etc*.[1]

The ionic conductivity of some solids can be increased by heterogeneous doping, which is carried out by mixing a solid (usually, a solid electrolyte) and a chemically inert, insoluble dispersed phase (most often, an insulator) and subsequent formation of interphase boundaries of the solid electrolyte/insulator type. Such composite materials are called dispersoids.[2] The interphase boundaries influence the transport properties of dispersoids. The enhancement of ionic conductivity was for the first time observed by Liang.[3] He demonstrated that the ionic conductivity of $LiI-Al_2O_3$ dispersoid is 50 times higher than that of pure LiI. Later on, this effect was confirmed for some other dispersoids[2] and heterostructures.[4] Thus, a new avenue of research emerged in the field of surface science, namely, surface ionics,[5,6] which has been intensively developed recently in connection with the development of new technologies.[7,8]

The surface phase transitions[9,10] substantially affect the ionic conductivity of polycrystalline solids. For instance, such factors as the grain boundary wetting transition and the formation of liquid-channel grain boundary structure in ceramic composites significantly increase the ionic conductivity.[11] High ionic conductivity of oxide layers with the liquid-channel grain-boundary structure, which are formed on the surface of metals under high-temperature corrosion conditions, was for the first time reported in Ref. 12 then in Refs 13 and 14. Accelerated mass transfer along intergranular liquid channels resulted in catastrophic degradation of metal.[15–19] Recently, composites with the liquid-channel grain-boundary structure[20–23] were used to design ion transport membranes with highly selective oxygen permeation that may appear to be an alternative to traditional ceramic membranes.[24–30]

The use of liquid-channel grain boundary nanostructures offers great prospects for the design of high-temperature nanomaterials.[31]

This review is devoted to the thermodynamics of grain boundary wetting and the mechanisms of formation of liquid-channel grain-boundary structures in ceramic materials. We systematized and generalized the experimental data and results of theoretical studies mainly obtained in the last 5 years in the field of research on oxygen permeation properties of (i) ion transport membranes with liquid-channel grain-boundary structures and (ii) oxide layers formed on the metal surface under high-temperature corrosion involving the liquid phase. It should be noted that oxygen permeation properties of conventional ceramic membranes have been considered in detail in reviews by Bouwmeester and Burggraaf,[25] Sunarso *et al*.[32] and Hashim *et al*.[33] The present review differs from them in that the

V V Belousov, S V Fedorov A A Baikov Institute of Metallurgy and Materials Science, Russian Academy of Sciences, Leninsky prosp. 49, 119991 Moscow, Russian Federation. Fax (7-499) 135 86 80, tel. (7-495) 718 16 55, e-mail: vbelousov@imet.ac.ru (V V Belousov), fedserv@rambler.ru (S V Fedorov)

Received 22 January 2011
Uspekhi Khimii **81** (1) 44 – 64 (2012); translated by S E Boganov

effect of the grain boundary wetting transition on the transport properties of ceramic materials, as well as the kinetic regularities of oxygen transfer processes in the recently produced solid oxide – oxide melt composite membranes with the liquid-channel grain boundary structure are considered for the first time.[20–23]

II. Thermodynamics of grain-boundary wetting in polycrystalline materials

1. Grain boundaries

A grain boundary is a transition region (about 1 nm wide) between two misoriented grains, or crystallites (Fig. 1). Since the grain contact region has a specific atomic structure different from the structure of a perfect crystal, the grain boundary properties can differ from the properties of the material in the bulk. Therefore, the grain boundary can be considered as a specific phase distinguished from the bulk by its structure and properties.

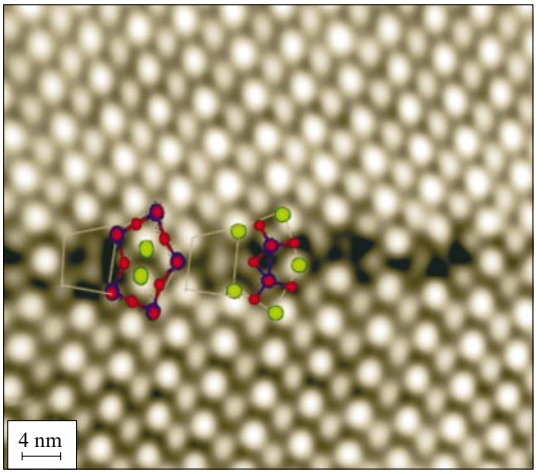


Figure 1. HR TEM image of a grain boundary in $SrTiO_3$ ceramics.[34]
Inset: the lattices at the grain boundary.

a. Geometric characteristics of grain boundaries

The grain boundary is the separation surface between two differently oriented crystallites. It can be described using the relative orientation of the interfaced crystallites and the orientation of the boundary surface relative to the crystal lattice of each grain provided that the inherent atomic structure of the grain boundary is left out of consideration. The corresponding grain boundary parameters are referred to as macroscopic ones. On the atomic level, the grain boundary is described by microscopic parameters characterizing (i) the displacement of the grains relative to one another at a given misorientation and the boundary orientation, as well as the specific location of the boundary relative to the lattice sites.[35] Generally, the grain boundary is characterized by 9 (5 macroscopic and 4 microscopic) crystallographic parameters or degrees of freedom.

Misorientation of grains. Misorientation of grains, *i.e.*, the mutual orientation of two neighbouring crystallites, is described by the angle of rotation (Ψ) of one crystallite

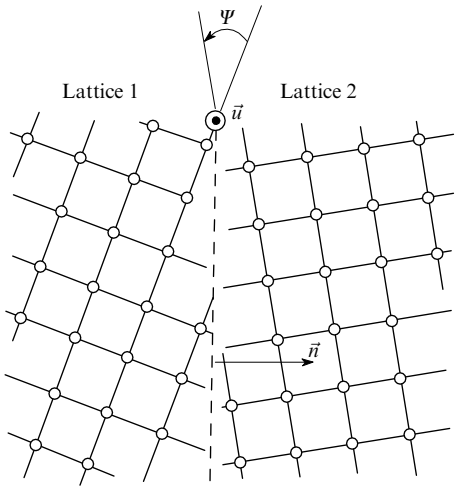


Figure 2. A grain boundary: a schematic.
The axis $\vec{u}$ is normal to the figure plane; the plane of the grain boundary is indicated by the dashed line; $\vec{n}$ is the normal to this plane.

relative to the other around the crystallographic axis $\vec{u}$ common to both crystallites, resulting in matching of their crystal lattices (Fig. 2). The angle Ψ is called the misorientation angle and the direction $\vec{u}$ is the misorientation axis. The vector $\vec{u}$ is chosen of unit length and can therefore be described by two components. In the general case, the grain misorientation is specified by three scalar parameters, of which one defines the angle Ψ and the other two define the misorientation axis $\vec{u}$. The three parameters specify the misorientation vector

$$\vec{\Psi} = \Psi \times \vec{u}. \tag{1}$$

Mutual rotation of two identical 3D lattices can be described by the matrix of rotation (so-called misorientation matrix). The relation

$$\vec{A} = \hat{R} \times \vec{B}, \tag{2}$$

is valid for any pair of parallel directions in two grains defined by two unit vectors $\vec{A}$ and $\vec{B}$.

Here $\hat{R}$ is the matrix of linear transformation with 9 coefficients, only 3 of which being independent. The misorientation angle Ψ and the misorientation axis $\vec{u}$ are uniquely determined by the matrix $\hat{R}$:

$$\vec{u} = \hat{R} \times {}'\vec{u}.$$

Here ${}'\vec{u}$ is the eigenvector $\hat{R}$. The misorientation angle Ψ is the angle between the vectors $[\vec{u} \times \vec{D}]$ and $\hat{R}[\vec{u} \times \vec{D}]$, where $\vec{D}$ is a vector non-collinear to $\vec{u}$.

Orientation of the grain boundary surface. A planar grain boundary is characterized by the unit normal to it $\vec{n}$ (see Fig. 2). Two degrees of freedom are associated with the orientation of the boundary surface. Probably, any curvilinear grain boundary can be approximated by a number of planar (on appropriate length scale) facets (Fig. 3 *a*). In this case, each facet should be characterized by its unit normal. It is sufficient to describe the boundary plane in terms of the lattice indices of one grain because in

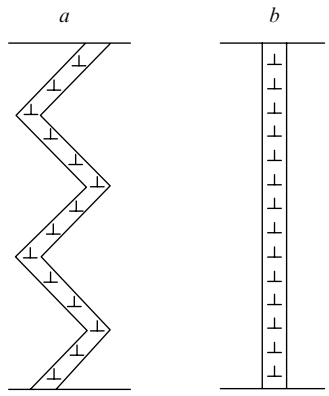


Figure 3. The dislocation structure of a grain boundary in a bicrystalline film.
(*a*) Faceted boundary, (*b*) flat symmetric tilt boundary.

the coordinate system of the second grain this plane is unambiguously indexed *via* the given grain misorientation, namely, if $\vec{n}_1$ and $\vec{n}_2$ are the normals to the boundary plane in the lattices of the first and second grain, respectively, from Eqn (2) we get

$$\vec{n}_2 = \hat{R} \times \vec{n}_1. \tag{3}$$

Microscopic grain boundary parameters. The formation of a grain boundary may involve not only mutual rotation of crystallites, but also their mutual displacement. A fixed displacement of one crystallite relative to the other is an identical transformation if the crystal is considered as a uniform continuous medium. However, a microscopic consideration taking into account a discrete crystal structure reveals that such a displacement results in a new grain boundary structure at the same macroscopic parameters (grain misorientation and the boundary surface orientation). In principle, the relative translation can be of any magnitude and direction, being associated with three macroscopic degrees of freedom.

The parameters $\vec{\Psi}$ and $\vec{n}$ to a great extent determine the physical properties of grain boundaries and serve as the basis for their classification. If $\vec{\Psi}$ and $\vec{n}$ are orthogonal (*i.e.*, the axis of rotation lies in the boundary plane), we have a tilt boundary (Fig. 3 *b*); if $\vec{\Psi}$ and $\vec{n}$ are parallel, one gets a twist boundary. Other mutual orientations of $\vec{\Psi}$ and $\vec{n}$ correspond to a mixed boundary. Methods of description of mixed boundaries have been considered in detail.[36]

b. The grain boundary energy

The most important physical parameter of a particular grain boundary is its specific energy (γ_{gb}), that is, the free energy per unit area of the boundary surface, which depends on the degree of grain misorientation, the thermal and mechanical prehistory, the chemical composition of the crystal, *etc*. The effect of the chemical composition manifests itself as two key factors, *viz*., the type of chemical bonds in the substance (covalent, ionic, *etc*.) and the ability to segregate impurities at grain boundaries.

Consider how the grain boundary energy depends on the degree of grain misorientation. With respect to the degree of grain misorientation, there are low-angle and high-angle grain boundaries. The former are formed by the edge dislocation walls (for tilt boundaries) or by screw dislocation walls (for twist boundaries) and their specific energies are comparable to the dislocation energy per unit area of the boundary surface,[37]

$$\gamma_{gb} = \gamma_0 \Psi (B - \ln \Psi), \tag{4}$$

where γ_0 and B are the parameters of the model chosen; γ_0 is calculated from the dislocation model and elastic constants; and B depends on the energy of atomic disorder inside the dislocation. Equation (4) quite well describes the boundaries up to $\Psi = 5-6^\circ$ (Fig. 4).

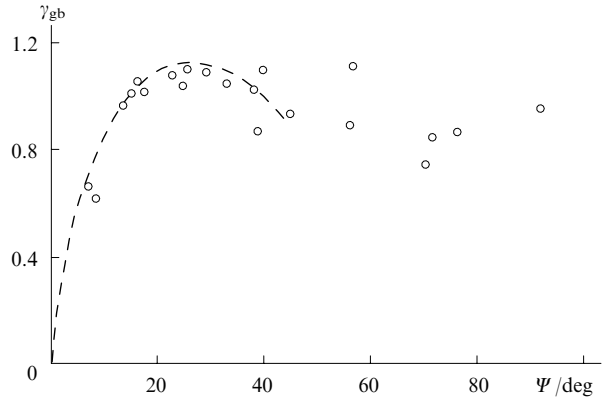


Figure 4. Energy of low-angle grain boundaries plotted *vs*. misorientation angle.[37]

Generally, the dependence of the energy of high-angle grain boundaries on the misorientation angle cannot be determined unequivocally. A characteristic feature of this dependence consists in the presence of sharp minima (Fig. 5) corresponding to the so-called special boundaries. In accordance with concepts of formal geometric crystallography, the structure of conventional grain boundaries is specified by the 0-lattice model,[38] whereas that of special boundaries is described by the coincident-site lattice model.[39, 40]

Based on the results of experimental observations for various systems (see, *e.g*., Refs 41–44), general regularities were established for relations between the grain boundary

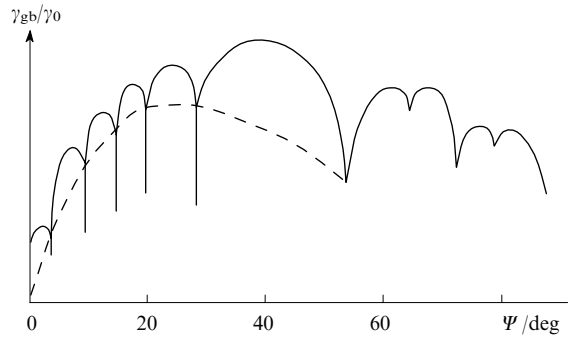


Figure 5. Relative energy of high-angle grain boundaries plotted *vs*. misorientation angle.

energy and structure. Namely, it was shown that the low-angle boundaries, irrespective of their type (tilt or twist boundaries), as well as special boundaries usually have low energies.

c. The coincident-site lattice model

Among geometrical models predicting the existence of special boundaries, the coincident-site lattice model was developed first. Using this model, it was shown that boundaries were classified as special ones only based on equality of the misorientation to specific, strictly fixed values of the parameters $\vec{u}$ and Ψ. In these cases, three-dimensional superlattices are formed by the coinciding sites of the grain lattices; thus, one deals with the coincident-site lattices. The parameters of the coincident-site lattice model include the misorientation angle Ψ and the volume fraction of coinciding sites Σ^{-1} (this is the reciprocal of Σ equal to the ratio of the unit cell volumes of the coincident-site lattice and the grain lattice).[45]

Geometrically, special boundaries are those characterized by relatively large particular values of Σ. Physically, special boundaries are those whose properties are different from the properties of conventional boundaries. Clearly, at rather large Σ values, the boundary periodicity has little effect on its properties. Opinions differ on the reasonable magnitude of the upper limit of Σ. According to a theory,[46] the key conditions for the existence of special boundaries are as follows:

— manifestation of the specific properties of special grain boundaries in particular intervals of misorientation angles and temperatures;

— a decrease in the special boundary – conventional boundary transition temperature with increasing Σ;† and

— exponential narrowing of the misorientation angle range corresponding to the existence of special boundaries at low temperatures with increasing Σ.

d. Phase transitions at grain boundaries

The special boundary preserves its specific properties as long as the depth of its potential profile determined by the total superimposition lattice exceeds kT (where k is the Boltzmann constant). Using the Lindemann criterion (the root-mean-square amplitude of thermal atomic vibrations at a temperature close to the melting point is equal to about one-tenth of the interatomic distance) and a relation between the total superimposition lattice constant and Σ, an expression was derived [47] for estimation of Σ_{max}, which is the limiting Σ value at a given temperature at which the boundary still remains special,

$$\Sigma_{max} \sim 25\,\alpha\,\frac{T_m}{T}, \tag{5}$$

where $\alpha < 1$ is a coefficient to account for the difference between the melting points of the crystal with the coincident-site lattice and a real crystal. According to Ref. 48, the coincident-site lattice boundary preserves its specific properties in a particular temperature range $T < T_0$:

$$T_0 = 25\,\alpha\,\frac{T_m}{\Sigma}. \tag{6}$$

From Eqn (6) it follows that at $\Sigma < 25$, this temperature range can extend up to the melting point of the crystal. Therefore, a special boundary – conventional boundary transition can occur at T_0.[49] Probably, within the approach considered, this should be a phase transition of the first order. This is substantiated by a fixed transition temperature and different crystallographic parameters of the boundary phases. The special boundary – conventional boundary transition is a specific kind of grain boundary transition. The phase transitions at grain boundaries were analyzed in detail [50–53] relying on the known studies.[9, 54, 55]

2. The grain boundary wetting

The Young equation describes the equilibrium conditions for a three-phase boundary (Fig. 6)

$$\gamma_{sg} = \gamma_{sl} + \gamma_{lg}\cos\theta, \tag{7}$$

where γ_{sg}, γ_{sl} and γ_{lg} are the surface tensions at the solid – gas, solid – liquid and liquid – gas interfaces, respectively; and θ is the contact angle. We also introduce the spreading coefficient S:

$$S = \gamma_{sg} - (\gamma_{sl} + \gamma_{lg}). \tag{8}$$

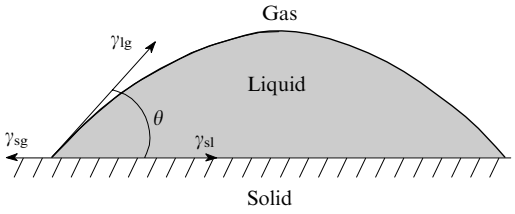


Figure 6. Profile of a liquid drop partially wetting a solid surface.

If $\theta > 0$, one has $S < 0$. The case $\theta = 0$ is called complete wetting. Here, one has $S = 0$. Under thermodynamic equilibrium, S cannot take positive values, because otherwise the solid – gas boundary surface cannot exist as it would be more preferable for it to be coated with a thin layer of liquid to reduce its surface energy from γ_{sg} to $\gamma_{sl} + \gamma_{lg}$. Obviously, all the quantities in Eqns (7) and (8) are some functions of temperature. Therefore, the following situation seems to be possible: the coefficient S increases with temperature until it becomes equal to zero at some temperature $T = T_w$. This phenomenon is called the wetting transition or the Cahn transition and the temperature T_w is the wetting transition temperature.

Cahn [9] showed experimentally and theoretically that the wetting transition can occur in the vicinity of the critical point. He considered a system $\alpha + \beta$ (its components exhibit limited solubility in each other) contacting a solid phase λ (Fig. 7). The two-phase region is confined by the binodal with the critical point C. Cahn established that, as the temperature approaches T_c, the energy of the α/β interphase

† Thus, only the boundaries with $\Sigma < \Sigma_{max}$ exhibit special properties at a given temperature. With decreasing temperature, the proportion of boundaries exhibiting special properties increases. At the same temperature, the boundaries with larger Σ values will exhibit the special properties in materials with higher melting points (T_m).

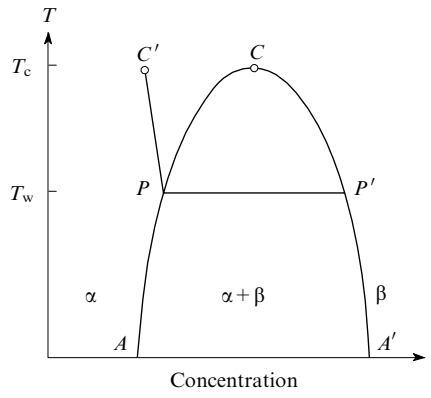


Figure 7. The solubility diagram of a binary system with limited solubility of components α and β in each other.[5]

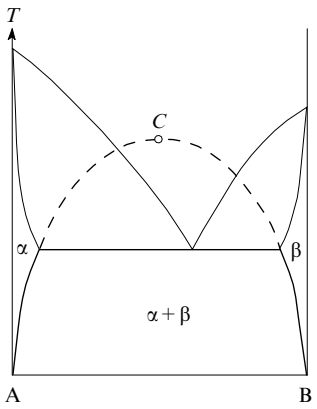


Figure 8. The state diagram with a 'virtual' critical point C.[5]

boundary decreases faster than the interphase energy difference between $\gamma_{\alpha\lambda}$ and $\gamma_{\beta\lambda}$. This means that there is a temperature T_w above which an interlayer of the phase β is necessarily present in the two-phase region between the vessel wall λ and the phase α. The wetting transition occurs at the temperature T_w (the conode PP'). Cahn also showed that under thermodynamic equilibrium a thin film of the phase β can also exist at the α/λ boundary beyond the two-phase region (see Fig. 7), *viz*., between the line PC' and the binodal segment PC. This phase transition was called the prewetting transition by Cahn.

The Cahn theory was repeatedly confirmed experimentally. For example, a mixture of cyclohexane and methanol has a critical point at 46 °C. Moldover and Cahn[56] experimentally established that the wetting transition takes place on approaching this critical point. As a result, a thin layer of methanol separating cyclohexane from the vessel wall appears. The transition is reversible: as the temperature decreases, the dewetting transition occurs and the layer disappears; raising the temperature again causes the formation of a methanol layer between cyclohexane and the vessel wall.

The Cahn theory can be generalized as follows.

1. The wetting transition is possible provided that the phases α and β are solid phases. It is necessary that the boundary energy $\gamma_{\alpha\beta}$ should tend to zero when the difference $(T-T_c)$ tends to zero. This phenomenon is called solid-phase wetting.[56]

2. The third phase λ is not required for the wetting transition to occur. A layer of the phase β can be formed at the phase α grain boundary provided that

$$\gamma_{\alpha\alpha} > 2\gamma_{\alpha\beta}. \tag{9}$$

3. If the mixing enthalpy of the components A and B is positive and sufficiently high, the critical point C can be 'virtual' (Fig. 8). In other words, it can be located above the liquidus line for the two-component system. It is necessary for wetting transition to occur that the energy $\gamma_{\alpha\beta}$ should tend to zero in the vicinity of such a 'virtual' critical point.

Cahn's studies on the possibility for wetting transitions to occur attracted much attention of theoreticians and experimentalists.[9, 57–59] Grain boundary wetting transitions in ceramic materials were extensively studied.[10, 11, 60–67] We will shortly dwell on the thermodynamics of the boundary wetting (Fig. 9). Under partial wetting of a grain boundary,

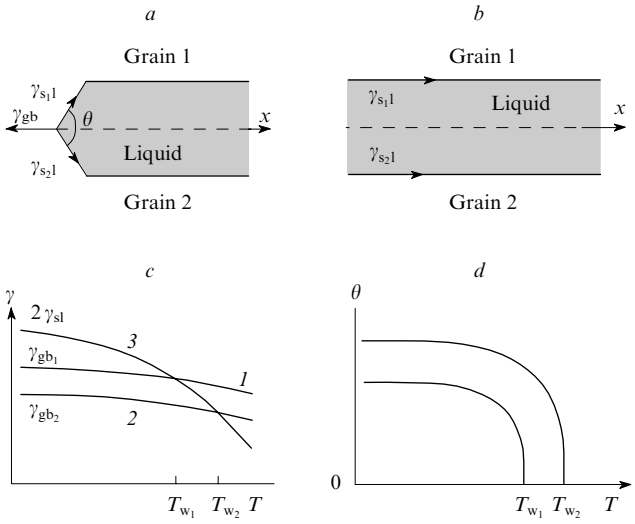


Figure 9. The diagrams of grain boundary wetting.[52]
(*a*) Partial wetting at $T_c < T_w$; (*b*) complete wetting at $T_c \geqslant T_w$; (*c*) temperature dependences of the surface tension: γ_{gb_1} (*1*), γ_{gb_2} (*2*) and $2\gamma_{sl}$ (*3*); (*d*) temperature dependences of the contact angle θ corresponding to curves (*1*) and (*2*) in Fig. 9 *c*.

two phases (a liquid and a solid one) are in contact. The contact angle θ at the point where the grain boundary contacts the liquid/solid interface is given by

$$\gamma_{gb} = 2\gamma_{sl}\cos\frac{\theta}{2}. \tag{10}$$

Consider a contact between two grains and the liquid phase. At $\gamma_{gb} < 2\gamma_{sl}$, the grain boundary is partially wetted by the liquid phase and $\theta > 0$ (see Fig. 9 *a*). If $\gamma_{gb} \geqslant 2\gamma_{sl}$, the grain boundary is completely wetted by the liquid phase and the contact angle $\theta = 0$ (Fig. 9 *b*). In this case, the grain boundary cannot exist in equilibrium with the liquid phase and is replaced by a thin layer of the liquid phase. The thermodynamic condition for wetting of the grain boundary has the form:[68]

$$\gamma_{gb} \geqslant 2\gamma_{sl}. \tag{11}$$

In some systems, transition from partial wetting of the grain boundary by the liquid phase to complete wetting can occur upon temperature variation. Consider the temperature dependences of the energies γ_{gb} and γ_{sl} (Fig. 9 *c*). If the plots of the dependences $2\gamma_{sl}(T)$ and $\gamma_{gb}(T)$ intersect, a grain boundary wetting transition occurs at the intersection temperature T_w. In this case, the contact angle θ gradually decreases with increasing temperature and becomes equal to zero at the wetting transition temperature T_w (Fig. 9 *d*). At temperatures above T_w, the contact angle remains equal to zero. In the phase diagram, this is shown by a line corresponding to the surface phase transition, *i.e.*, a conode of the grain boundary wetting transition at T_w in the region of equilibrium between the solid and liquid phases. Above this line, the grain boundary cannot exist in equilibrium with the liquid phase and should disappear. Such a 'disappearance' at T_w is just the grain boundary wetting transition. Above T_w, the liquid phase forms a layer separating the solid grains (crystallites).

If grain boundaries have different energies, the wetting transition occurs at different temperatures, *viz.*, the higher the energy γ_{gb} the lower T_w. The temperature dependences of the contact angle for two grain boundaries with different energies are schematically shown in Fig. 9 *d*. The energy of the high-angle boundaries is higher than that of the special and low-angle boundaries; therefore; they are wetted at lower temperatures compared to the last two types of boundaries.

3. Grain boundary wetting in ceramic materials

It is experimentally established that the grain boundary wetting transition occurs in some ceramic materials.[11,60–67,69,70] Thin films of Al, Al_2O_3 and $(Al_2OC)_{1-x}\cdot(AlN)_x$ were revealed at grain boundaries and triple junctions of TiB_2 grains[60] upon the interaction of dense TiB_2 ceramics (96%–98% of theoretical density) with liquid aluminium in air at 980 °C for 7 h (Fig. 10). It was established that most of grain-boundary thin films and inclusions at triple grain junctions of TiB_2 contain metallic aluminium, while minority of those include oxide, oxycarbide and nitride phases [α-Al_2O_3, β-Al_2O_3 and $(Al_2OC)_{1-x}(AlN)_x$].

Fujimoto and Kingery[61] studied the microstructure of ceramic capacitors based on $SrTiO_3$ at various stages of heat treatment by high-resolution transmission electron microscopy (HR TEM). Ceramics for the capacitors was prepared by liquid-phase sintering of powdered $SrCO_3$, TiO_2, Nb_2O_5, SiO_2 and Al_2O_3 at 1450 °C (above the melting point of $SrTiO_3-TiO_2$ eutectic) for 3 h followed by heat treatment in the presence of flux (powdered mixture of Bi_2O_3, PbO, CuO and B_2O_3) at 1000 °C for 30 min and subsequent cooling at different rates. It was found that the flux wetted the $SrTiO_3$ grain boundaries. Under slow cooling of samples, the reverse 'dewetting' transition occurred and the liquid phase gathered at triple junctions of grains. Analogous phase transitions were also observed for the ceramic composites $ZnO-Bi_2O_3$,[62–65] $Bi_2CuO_4-Bi_2O_3$,[66,67] $Si_3N_4-SiO_2$ (Refs 69, 70), *etc.*

Thin intergranular films formed as a result of grain boundary wetting can have unique properties. For instance, Matsuoka[63] supposed that specific electrical properties of varistors based on ZnO are due to the presence of thin intergranular films at boundaries of Bi_2O_3-enriched grains (Fig. 11). Gambino *et al.*[64] showed that in ZnO-based varistors containing ~0.5 mol.% Bi_2O_3 and 0.5 mol.% Co_2O_3, the ratio of wetted and non-wetted grain boundaries changes from 0 at temperatures below the melting point of $ZnO-Bi_2O_3$ eutectic (750 °C, Ref. 71) to 88% at 1140 °C. Olsson and Dunlop[65] distinguished two types of grain boundaries in varistors, *viz.*, active and passive ones. The former type of boundaries contains intergranular films about 2 nm thick, whereas the latter type does not contain intergranular films.

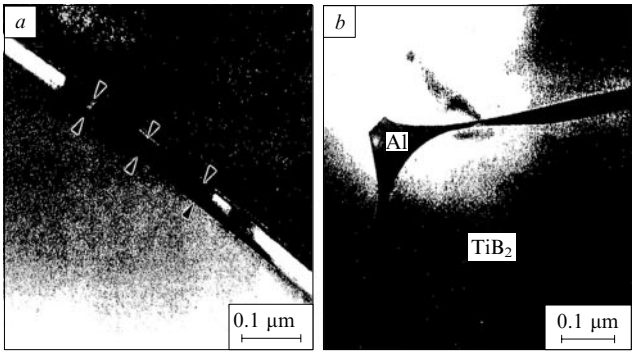


Figure 10. Photomicrographs illustrating wetting of a grain boundary (*a*) and triple junctions (*b*) in TiB_2 by metallic Al melt.[60] The intergranular film thicknesses are indicated by arrows.

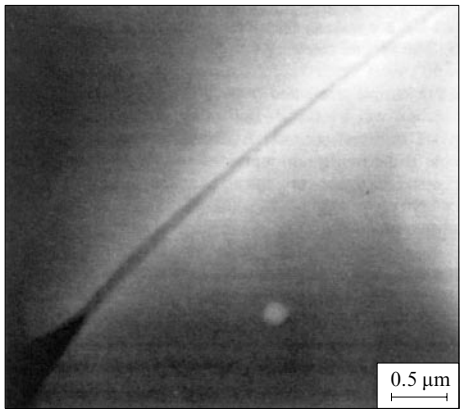


Figure 11. Photomicrograph of intergranular film in $ZnO-Bi_2O_3-Co_2O_3$ ceramic varistor.[65]

Wetting of grain boundaries by eutectic melt was revealed in the system $Bi_2CuO_4-Bi_2O_3$.[66,67] The authors investigated the microstructure of $Bi_2CuO_4-Bi_2O_3$ composites preheated to a temperature above the eutectic melting point (770 °C) and then quenched in air. Typical microstructure of these composites quenched from 780 °C is shown in Fig. 12 *a,b*. Wetting of triple junctions and some Bi_2CuO_4 grain boundaries is seen. The presence of thin intergranular films (Fig. 12 *c*) represents a proof for wetting of grain boundaries in this composite.

Thin intergranular films were also found in other ceramic materials, for instance, silicon nitride Si_3N_4.[69,70] The existence of amorphous SiO_2 film along grain boundaries is necessary for the formation of dense Si_3N_4. Kleebe *et al.*[69] showed that the amorphous films are present on all

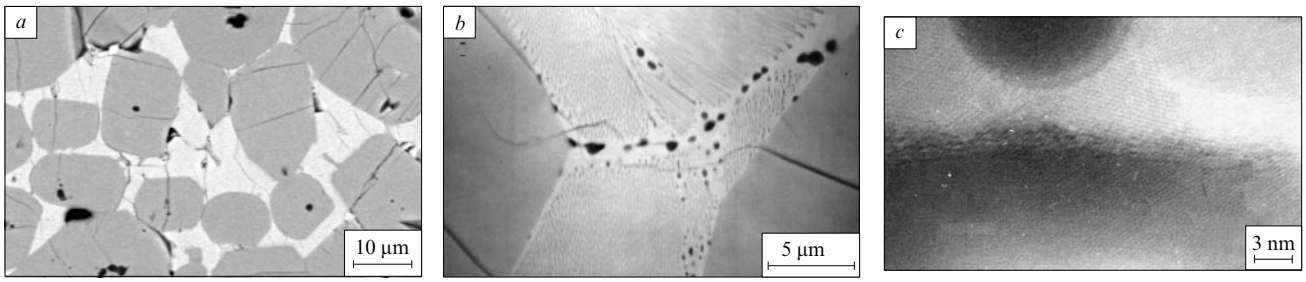


Figure 12. HR TEM images of the microstructures of $Bi_2CuO_4 - Bi_2O_3$ (20 mass %) composite quenched from 780 °C (*a*) and a wetted junction in the composite (*b*); HR TEM image illustrating the existence of a thin intergranular film (1 – 2 nm thick) in this composite (*c*).[67] The Bi_2CuO_4 phase, eutectic and pores are shown in grey, white and black, respectively.

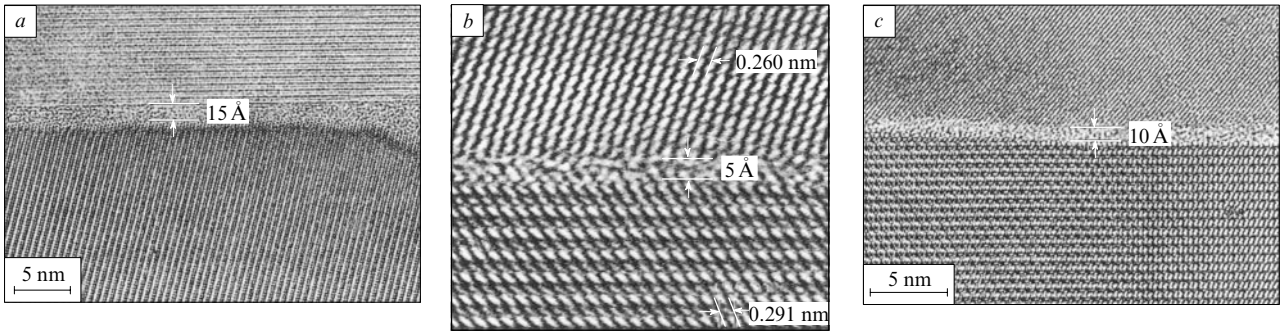


Figure 13. HR TEM images of thin intergranular films in Si_3N_4.[70] (*a* – *c*) Different grain misorientation angles. The vertical arrows show the intergranular film thicknesses, the horizontal arrows indicate the interplanar spacing.

high-angle grain boundaries in silicon nitride, except special boundaries. A HR TEM study [72] revealed thin intergranular films in various ceramic materials (see Fig. 12 *c* and 13); their thicknesses were measured.[13, 69, 70, 73 – 79] It was established that the thickness of an intergranular film depends only slightly on the misorientation angle. An exception is provided by low-angle and special grain boundaries at which no intergranular films were detected.

Intergranular films in ceramic material can be formed during liquid-phase sintering. Examples are provided by materials based on silicon nitride, varistor materials based on zinc oxide and materials for alumina substrates. In glass-ceramic materials, the formation of intergranular films is due to incomplete crystallization of glasses. In such practically valuable materials as ceramics for sealing of nuclear waste [76] or ceramics based on tetragonal zirconia,[77] intergranular films are formed by impurities present in the starting substances (impurity segregation).

4. Equilibrium thickness of intergranular wetting films in ceramic materials

Can thin intergranular wetting films have equilibrium thickness in the ceramic materials? Clarke attempted to answer this question.[80] He suggested two approaches to solve this problem. They are based on estimation of the boundary energies and on the balance of forces acting normal to the boundary. Clarke's study showed that there is an equilibrium thickness of intergranular film of ~ 1 nm. The stable thickness of the film is determined by two competing interactions, *viz*., attraction (van der Waals dispersion interaction) of grains and their repulsion (steric interaction which depends on the structure of the liquid present in the intergrain space).

Now we will dwell on the approach based on estimation of the boundary energies. To get a general description of the interphase region, we consider the phases and geometry shown in Fig. 14. An analysis of the stability and structure of the interface between two phases, α and λ, existing in equilibrium with the third (intermediate) phase β was carried out by Widom [81, 82] within the framework of the classical (van der Waals) theory of liquids. However, Widom (and more recently, de Gennes [83]) ignored the effect of long-range forces, *e.g*., the van der Waals dispersion forces.

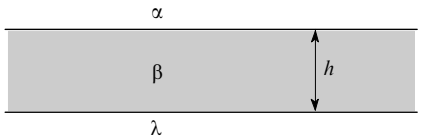


Figure 14. The boundary phase β of thickness *h* between the phases α and λ.

The analysis performed by Widom is based on the assumption that the boundary energies (γ) in the bulk phases obey the Antonov rule [84]

$$\gamma = \gamma_{\alpha\beta} + \gamma_{\beta\lambda} . \qquad (12)$$

Assuming that the phase β is in equilibrium with the phases α and λ, the energy of the α/λ interface reaches a minimum value if this interface includes a layer of the phase β irrespective of its volume fraction (see Fig. 14). As the volume fraction of the phase β decreases, the thickness of the layer of the phase β continuously decreases down to a value of the order of the characteristic coherence length (ξ). In accordance with the statistical thermodynamics approach,[81] the interface can be considered diffuse and having an excess energy density compared to the energy density at some distant point. Widom represented this energy density difference as the function $\exp(-|z|/\xi)$, where z is the distance from the boundary. Therefore, when the thickness, h, of the layer of the β phase becomes microscopically small, the energy is given by

$$\gamma = A\gamma_\infty e^{-h/\xi}, \tag{13}$$

where A is the surface area of the interface and γ_∞ is the interface energy at $h = \infty$.

In accordance with the classical theory of liquids it is assumed that the phase β of microscopic thickness h has an excess energy per unit area. Then, the total energy equals the sum of the boundary energies [see Eqn (12)] of sufficiently separated phases α and λ, which is independent of the distance h, augmented with a term describing the additional boundary energy [see Eqn (13)], which depends on h and arises at relatively short distances between the phases α and λ,

$$\gamma(h) = \gamma_\infty\left(1 + e^{-h/\xi}\right). \tag{14}$$

As mentioned above, the statistical thermodynamics approach ignores long-range interactions such as van der Waals interactions. To account for these interactions, de Gennes[83] suggested an equation of energy balance with an additional term

$$\gamma(h) = \gamma_\infty\left(1 + e^{-h/\xi}\right) + \gamma_{lrf}, \tag{15}$$

where γ_{lfr} is the contribution of long-range interactions

$$\gamma_{lfr} = -\frac{H}{12\pi h^2},$$

H is the Hamaker constant.

Measurements of the interaction force between two mica plates separated by distances down to about 1 nm showed that this expression is valid even for such short distances.[85–88] Differentiation of Eqn (15) gives

$$h^3 e^{-h/\xi} = \frac{H\xi}{6\pi\gamma_\infty}. \tag{16}$$

The second differentiation with respect to h shows that the energy is minimum and, hence, the system is stable at $h > 3\xi$. The equation relating the equilibrium film thickness to the parameters H, γ and ξ has the form

$$\frac{h}{\xi} = \ln\frac{162\pi\gamma_\infty\xi^2}{H} + \ln\left(\frac{h}{3\xi}\right)^3. \tag{17}$$

Taking into account the approximation that $h > 3\xi$ (in this case, the second term on the right side is small), the equation for the equilibrium film thickness can be written as follows

$$h \approx \xi\ln\frac{162\pi\gamma_\infty\xi^2}{H}. \tag{18}$$

The interface energy γ_∞ is comparable with the expression kT/ξ^2 in order of magnitude. Therefore, the equilibrium thickness of the film formed by the phase β at the boundary is given by

$$h \approx \xi\ln\frac{162\pi kT}{H}. \tag{19}$$

It should be noted that this thermodynamic approximation is rough.

Now we will consider the second approach based on the balance of forces acting normal to the surface of a thin intergranular film. To ensure stability of the thickness of the equilibrium intergranular film, it is necessary that the sum of forces acting normal to its surface be equal to zero,[89] *i.e.*

$$P + P_c + \Pi = 0, \tag{20}$$

where P is the external pressure, P_c is the capillary pressure and Π is the disjoining pressure. The concept of disjoining pressure was introduced by Derjaguin *et al.*[90] to designate the total effect of the forces capable of acting through the layer of the liquid intergranular phase. Generally, the following interactions contribute to the disjoining pressure

— van der Waals dispersion forces (Π_{disp}),
— interaction related to the electric double layer (Π_{edl}),
— interaction due to adsorption of solute on the grain surfaces (Π_{ads}),
— hydrogen bond forces (Π_{hb}), and
— structural or steric interaction (Π_{sr}).

Thus, the following expression can be written formally

$$\Pi = \Pi_{disp} + \Pi_{edl} + \Pi_{ads} + \Pi_{hb} + \Pi_{sr}. \tag{21}$$

Detailed consideration of the balance of forces acting on the film assumes that these forces are those acting between two flat parallel surfaces of adjacent grains through a layer of the liquid intergranular phase. Since there is no experimental proof that the interactions caused by the adsorption of solute, formation of the electric double layer or hydrogen bonds do occur in multiphase ceramic materials at high temperatures, Clarke[89] suggested ignoring them. If this simplifying assumption is accepted, the resultant force acting through a thin intergranular film normal to the film surface is given by

$$P + P_c + \Pi_{disp} + \Pi_{sr} = 0. \tag{22}$$

The dispersion interaction. The dispersion (van der Waals) forces between individual atoms and molecules are inversely proportional to the seventh power of the distance between them, thus being short-range forces. In contrast, the dispersion force between solid phases acts over longer distances and changes slower with the distance as was shown for the first time by Hamaker.[91] Dzyaloshinskii, Lifshitz and Pitaevskii[92] applied an approach based on the Lifshitz quantum field theory to analysis of the London dispersion force between two interacting phases separated

by a third phase. The result obtained for two flat parallel plates (see Fig. 14) has the form

$$\Pi_{\text{disp}} = \frac{\hbar}{8,\pi^2 h^3} \int_0^{\infty} \sum_{n=1}^{\infty} \frac{1}{n^3} \left[\left(\frac{\varepsilon_\alpha - \varepsilon_\beta}{\varepsilon_\alpha + \varepsilon_\beta} \right) \frac{\varepsilon_\lambda - \varepsilon_\beta}{\varepsilon_\lambda + \varepsilon_\beta} \right] \mathrm{d}\xi, \tag{23}$$

where $\varepsilon_j = \varepsilon_j(\mathrm{i}\omega)$ is the dielectric constant of the jth phase depending on the imaginary frequency $\mathrm{i}\omega$ and $\hbar$ is the Planck constant divided by 2π. This equation shows that the dispersion force can be either attractive or repulsive depending on the relative values of the dielectric constants of the three phases (the dispersion force is repulsive at $\varepsilon_\alpha > \varepsilon_\beta > \varepsilon_\lambda$). If grains on both sides of the intergranular phase β are identical, Eqn (23) is reduced to the simpler expression

$$\Pi_{\text{disp}} = \frac{\hbar}{8,\pi^2 h^3} \int_0^{\infty} \sum_{n=1}^{\infty} \frac{1}{n^3} \left(\frac{\varepsilon_\alpha - \varepsilon_\beta}{\varepsilon_\alpha + \varepsilon_\beta} \right)^2 \mathrm{d}\xi = \frac{H_{\alpha\beta\alpha}}{6\pi h^3}. \tag{24}$$

In this case (symmetrical system), the dispersion force is always attractive irrespective of the nature of the materials forming the grain boundary. It is noteworthy that this equation has the form predicted by Hamaker.[91] Therefore, in the absence of external pressure and capillary pressure, thin intergranular films are unstable against the attractive force caused by dispersion interactions if there is no repulsive structural (steric) interaction that counterpoises the long-range van der Waals force.

The structural component of the disjoining pressure. It is assumed that, if the thickness of the intergranular phase is microscopically small, the liquid phase has a structure with fluctuating orientational order near each grain (epitaxy) rather than a random structure as could be expected for the bulk liquid phase. If the correlation length related to orientational fluctuation is ξ, the orientational order due to the influence of neighbouring grains on the structure of the liquid phase extends into the depth of the intergranular phase to a distance of about ξ. Clarke[89] assumed that the orientational order depends only on the coordinate normal to the boundary. It is believed that ordering is due to the fact that the first monomolecular layer of the liquid phase surrounding each crystalline grain predominantly adopts epitaxial arrangement on the grain surfaces. To calculate the structural component of the disjoining pressure, Clarke used the mean field approximation in which orientational ordering across the boundary is represented by the scalar quantity $\eta(x)$. Taking into account the above assumptions, the free energy density in the liquid phase can be expressed as follows:

$$g = g_0 + \left(a\eta^2(x) + b\eta^3(x) + c\eta^4(x) + \ldots \right) + K \left(\frac{\mathrm{d}\eta(x)}{\mathrm{d}x} \right)^2, \tag{25}$$

where K is a constant.

This equation known as the Cahn–Hillard[93] or Ginzburg–Landau[94] equation consists of three parts. The first part, the term g_0 is the free energy density in the massive liquid (not in a film) with disordered structure. The second part is an expansion of the order parameter $\eta(x)$ into a power series. The third part of the equation is so-called gradient energy, it determines the contribution corresponding to interactions of neighbouring molecules. Symmetry of the grain boundary region and, thus symmetry of the order parameter determines the condition $b = 0$. The constant c is small in comparison with a, therefore the term including $\eta^4(x)$ can be neglected. As a result, the density of the excess free energy is expressed by the simpler formula

$$g = g_0 + a\eta^2(x) + K \left(\frac{\mathrm{d}\eta(x)}{\mathrm{d}x} \right)^2. \tag{26}$$

Based on this equation, the functional of the excess free energy per unit surface area of the boundary can be expressed as

$$\Delta G = \int_{-h/2}^{h/2} (g - g_0)\mathrm{d}x. \tag{27}$$

Once the function ΔG_{eq} minimizing this functional is defined, the structural contribution to the disjoining pressure can be found from the following equation:

$$\Pi_{\text{sr}} = \frac{\mathrm{d}(\Delta G_{\text{eq}})}{\mathrm{d}h}. \tag{28}$$

To determine the equilibrium thickness of the intergranular film, it is necessary to establish conditions under which the functional (27) reaches a minimum value. A solution to this problem is given by the following expression for the excess free energy per unit area:

$$\Delta G_{\text{eq}} = 2(\alpha K)^{1/2} \eta_0^2 \operatorname{cth} \left(\frac{(\alpha/K)^{1/2} h}{2} \right) \tag{29}$$

provided that the grains on both sides of the boundary are disordered in such a manner that the orientational orderings of the first monolayers of the intergranular phase are opposite, *i.e.*

$$\eta_0 = \eta\left(\frac{h}{2}\right) = -\eta\left(-\frac{h}{2}\right).$$

The contribution of the disjoining pressure is obtained using Eqn (28)

$$\Pi_{\text{sr}} = \frac{\mathrm{d}(\Delta G_{\text{eq}})}{\mathrm{d}h} = -\frac{\phi_0}{\sinh^2(h/2\,\xi)}, \tag{30}$$

where

$$\phi_0 = a\eta_0^2,$$

$$\xi = (aK)^{1/2}.$$

If the thickness of the intergranular liquid phase is larger than the characteristic correlation length ($h > \xi$), the contribution of the disjoining pressure can approximately be represented in the form

$$\Pi_{\text{sr}} = -4\,\phi_0\,\mathrm{e}^{-h/\xi}. \tag{31}$$

Thus, this model predicts repulsive character [minus sign before the right-hand side of Eqn (31)] of the structural disjoining pressure, which is necessary to counterpoise the

van der Waals attraction between grains. Substituting the values expressed by (24) and (30) into Eqn (22), one gets the total force per unit area acting on the thin intergranular liquid film existing in equilibrium:

$$P + P_c + \frac{H}{6\pi h^3} - 4a\eta_0^2 e^{-h/\xi} = 0. \quad (32)$$

In the absence of external and capillary pressures, the equilibrium thickness of the intergranular liquid film determined from Eqn (33) is

$$\frac{H}{6\pi h^3} = 4a\eta_0^2 e^{-h/\xi}. \quad (33)$$

This equation derived on the basis of the balance of forces is analogous to Eqn (16) based on the statistical thermodynamics approach. Using two different continuum approaches (one based on the balance of forces acting normal to the intergranular liquid film and the thermodynamic approach), Clarke [89] showed that there exist conditions under which films of intergranular phases may have the equilibrium thickness. The thickness of intergranular films calculated from balance of forces agrees with that obtained by HR TEM for films in ceramic materials (1–2 nm). However, the validity of Clarke's calculations within the framework of the continuum theory of surface forces casts some doubt. Deryagin *et al.*[90] demonstrated that on the length scale less than 1.5 nm the continuum approach is of limited use and, therefore, quantitative estimate are not reliable.

A key issue is the nature of formation of thin intergranular films in ceramic materials. Are these films wetting or adsorptive? Most probably, one deals with adsorptive films formed at grain boundaries in equilibrium with the liquid phase at high temperature (Fig. 15). Possibly, such films remain at grain boundaries after reverse 'dewetting' transition and gathering of the intergranular wetting liquid to triple junctions of grains and pores upon cooling the ceramics. This hypothesis is supported by the fact that the compositions of intergranular films and wetting liquid localized at the triple and quadruple junctions of grains in $ZnO-Bi_2O_3$,[95–97] $Al_2O_3-CaO\cdot SiO_2$ (see Ref. 98) and some other ceramic materials are considerably different.

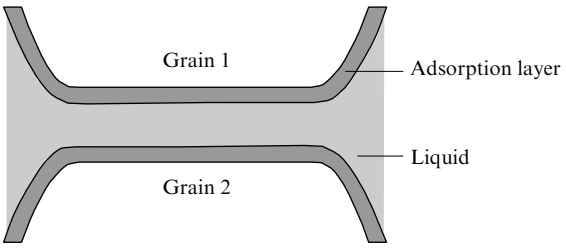


Figure 15. The structure of the intergranular channel.

From the aforesaid it follows that the grain boundary wetting transition can occur in ceramic composites at the melting point of eutectic. It results in composites consisting of solid grains and liquid intergranular channels.

III. The liquid-channel grain-boundary structures

Penetration of eutectic melt along grain boundaries into CuO-based ceramics coated with a layer of Bi_2O_3 powder was studied.[99] At 770 °C (melting point of the $Bi_2O_3-Bi_2CuO_4$), intense penetration of the eutectic melt along the CuO grains boundaries was observed (Fig. 16). The thickness of the intergranular layer depends on the amount of penetrant and can reach a few micrometres. It results in the formation of liquid-channel grain-boundary structures. These structures are also formed on melting of grain boundaries in ceramic materials.[13–15]

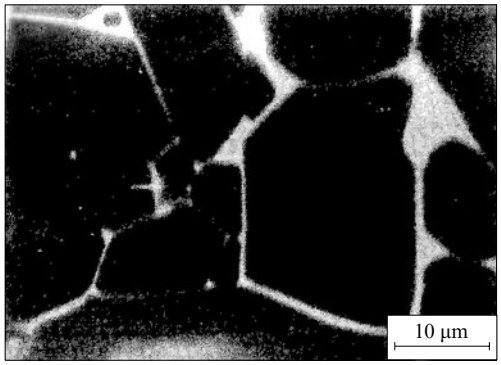


Figure 16. Microstructure of CuO ceramics heat-treated in contact with Bi_2O_3 in air (slice).[99]

With respect to their composition and structure, the liquid-channel grain-boundary structures are heterogeneous. Odelevskii [100] pointed out that there are two regimes of organization of heterogeneous structures, *viz.*, a matrix regime and a statistical one. A distinctive feature of the matrix distributed structures is that, among two or more components, one of them always forms a continuous matrix no matter how small is its volume. The liquid-channel grain-boundary structures should be attributed to the matrix distributed structures because the liquid phase forms a continuous matrix along grain boundaries (see Fig. 16).

Now we will dwell on possible mechanisms of formation of the liquid-channel grain-boundary structures.[101–105] In some cases, grooves characterized by a specific value of the dihedral angle θ (Fig. 17) are formed upon contact of the solid and liquid components at places where grain bounda-

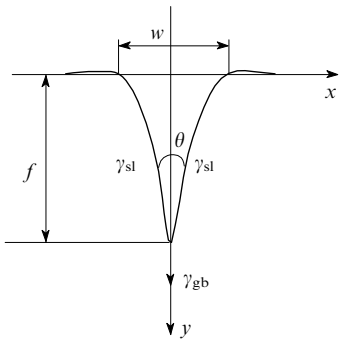


Figure 17. The profile of a grain-boundary groove produced during liquid-phase etching.[101]

ries access the surface. The θ value is related to the surface tensions of grain boundaries and the crystal–liquid boundary by equilibrium condition at the top of the groove [see Eqn (10)]. The growth mechanisms of the grain-boundary grooves under liquid-phase etching conditions can be different. We will consider etching by saturated and unsaturated solutions. In the former case, the development of a groove is due to the influence of capillary forces as in the case of thermal etching except the possibility of rapid mass transfer due to the presence of the liquid phase. Using the Mullins theory,[101] this process can be described by diffusion of atoms through the liquid phase. This procedure was carried out many times. An increase in the width (w) and depth (f) of the groove is proportional to $\tau^{1/3}$ (τ is the time of etching). Calculations and experimental results showed[103] that the maximum growth rate of the groove amounts to ~ 0.5 mm h^{-1} in this regime.

The growth of a groove in an unsaturated solution occurs under the influence of a concentration gradient. Two limiting situations are possible. First, the process can proceed in the kinetic regime ($w \sim \tau$, $f \sim \tau$) when the groove growth rate is controlled by the grain dissolution and the diffusion transfer is fast. Second, the process can proceed in the diffusion regime ($w \sim \tau^{1/2}$, $f \sim \tau^{1/2}$) when the groove growth rate is controlled by the diffusion through the liquid phase and dissolution is fast. The maximum rate of the groove growth in the diffusion regime amounts to several millimetres per hour.[104]

The feasibility to reach high rates of groove deepening in the kinetic regime was considered by Fradkov.[105] It was shown that for narrow grooves, the vertex moves much faster than the banks, it resembles the opening scissors. The groove deepening rate (v) is related to the dissolution rate of a flat solid surface (v_0) by the relation

$$v = \frac{v_0}{\sin(\theta/2)} .$$

However, an estimation using this expression showed that high groove deepening rates (for instance, a few centimetres per minute) are physically impossible. They can be attained only at $\theta \simeq 0.2'$. The situation is changed with increasing v_0. This can occur if the groove deepening rate is controlled by the kinetics of channel opening at the vertex rather than the kinetics of widening of the banks.[99] As a result, a liquid-phase grain-boundary structure is formed in the polycrystalline solid (see Fig. 16).

The possibility of existence of a liquid-channel grain-boundary nanostructure, which can be formed in the two-phase region by wetting of low-angle grain boundaries by a chemically compatible melt, was considered. The surface tension at the solid–melt interface surface should not be high.[106, 107] Consider the thermodynamic feasibility of wetting of low-angle grain boundaries.[108] According to Eqn (4), the energy γ_{gb} increases with increasing the misorientation angle Ψ and reaches a maximum value of $\gamma_{gb\,max}$. If the angle Ψ corresponding to $\gamma_{gb\,max}$ is denoted as Ψ_{max}, Eqn (4) can be transformed as follows:[109]

$$\frac{\gamma_{gb}}{\gamma_{gb\,max}} = \frac{\Psi}{\Psi_{max}} \left(1 - \ln \frac{\Psi}{\Psi_{max}} \right) . \qquad (34)$$

An estimation for low-angle grain boundaries ($10'' \leqslant \Psi \leqslant 1^\circ$) in ceramic materials using relation (34) showed that $1 < \gamma_{gb} < 150$ mJ m^{-2}, being equal to 10^3 mJ m^{-2} at $\Psi_{max} = 30^\circ$. Thus, the thermodynamic condition (11) for wetting of low-angle boundaries is met at $0.5 \leqslant \gamma_{sl} \leqslant 75$ mJ m^{-2}. These γ_{sl} values are typical of lyophilic colloids.[106] The formation of the liquid-channel grain-boundary nanostructure can be explained as follows. Wetting of high-angle grain boundaries by eutectic melts is established in the two-phase region for many systems (point C in Fig. 18).[13, 110] The energy γ_{sl} decreases with further increase in temperature. At $\gamma_{sl} < 75$ mJ m^{-2}, wetting of low-angle grain boundaries by the chemically compatible melt (point D in Fig. 18) and formation of the liquid-channel grain-boundary nanostructure become feasible.

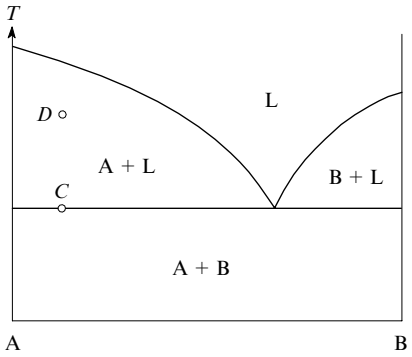


Figure 18. Phase diagram of the system A–B.[31] 'L' denotes the liquid phase.

IV. Accelerated mass transfer in ion-transport membranes and oxide layers

1. The ion-transport membranes

The development and fabrication of ion-transport membranes possessing high mixed ionic–electronic conductivity is a promising area in membrane materials science.[24–26, 111–191] The interest in the studies of such membranes is first of all due to the prospects for their applications in power engineering (in fuel cells), chemical industry (in ceramic membrane reactors for methane conversion into syngas), nano- and microelectronics (in separators for production of ultrapure oxygen and in other electrochemical devices).

A number of materials (perovskites, BIMEVOX and solid electrolyte/noble metal cermets) exhibit high mixed ionic–electronic conductivity;[27–30] however, they have some essential shortcomings (high fragility, insufficient thermodynamic and/or mechanical stability, high cost, *etc.*) hampering practical application. Therefore, the design of alternative membrane materials is an important problem in materials science. Composites with liquid-channel grain-boundary structure may appear to be an alternative to traditional membrane materials.[20–23, 192, 193] Below we will consider mass transfer processes in (i) polycrystalline solids with participation of the liquid phase taking the best studied $BiVO_4-V_2O_5$ ion-transport membranes with the liquid-channel grain-boundary structure as examples and (ii)

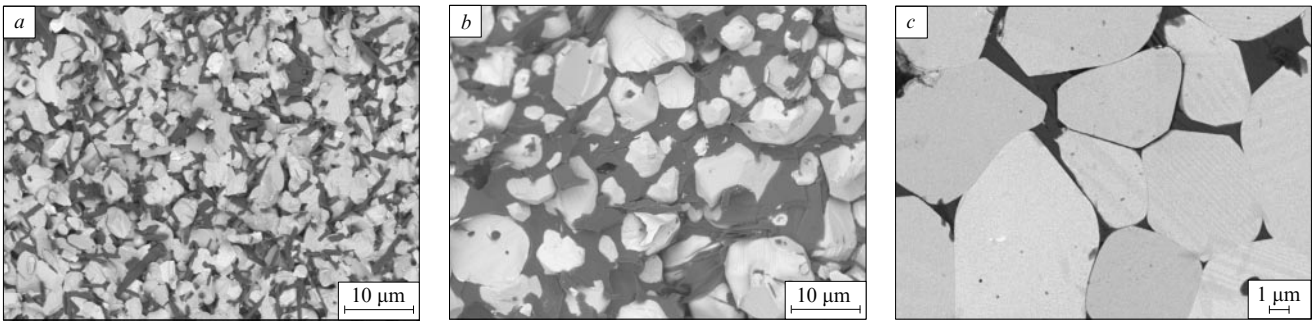


Figure 19. Microstructures of $BiVO_4-V_2O_5$ (10 mass %) composites.[22]
(*a*) A sample sintered at 600 °C; (*b*, *c*) samples cooled from 640 °C; a chip and a slice, respectively.

oxide layers formed on the copper surface under high-temperature gas corrosion.

The charge and mass transfer in ion-transport membranes based on $BiVO_4-x\,V_2O_5$ [x = (5, 7, 10, 12) mass %] composites with the liquid-channel grain-boundary structure formed by grain boundary wetting were studied.[20, 22] Samples with the liquid-channel grain-boundary structure were produced by heating sintered ceramic composites (Fig. 19 *a*) to the melting point of the $BiVO_4-x\,V_2O_5$ eutectic (640 °C, see Fig. 20).[194] The samples obtained (Fig. 19 *b*,*c*) were of high density and plasticity.[195]

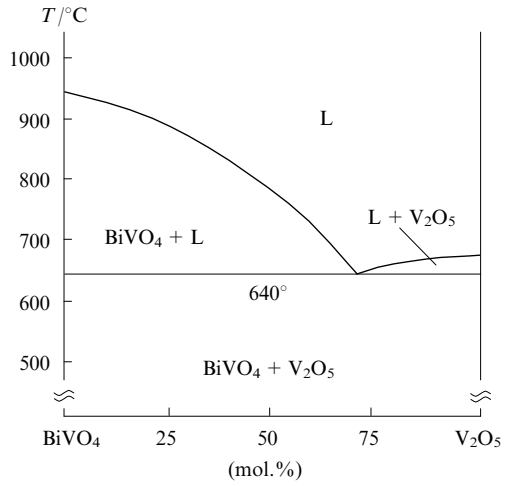


Figure 20. Phase diagram of the system $BiVO_4-V_2O_5$.[194]

The conductivities of the composites are plotted *vs.* temperature in Fig. 21. The temperature dependences of the conductivities of $BiVO_4$ and V_2O_5 are shown for comparison.[196, 197] The composite conductivities increase with increasing the V_2O_5 concentration. The conductivity decreases in the temperature range 600–635 °C, which is typical of V_2O_5 in the premelting region (curve *6* in Fig. 21).[22, 198–209] On further heating, the eutectic melts at 640 °C and the conductivity increases abruptly. This increase in the conductivity is caused by the formation of the liquid-channel grain-boundary structure in the composite (see Fig. 19 *b*,*c*). The isothermal time dependence of the conductivity of the $BiVO_4-V_2O_5$ (10 mass %) composite is

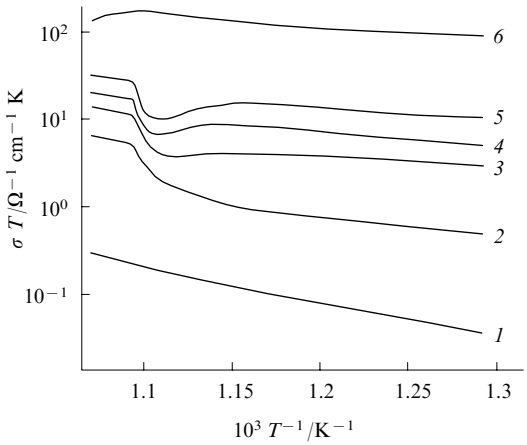


Figure 21. Conductivity-*vs.*-temperature plots for $BiVO_4$ (*1*), $BiVO_4-x\,V_2O_5$ (*2*–*5*) and V_2O_5 (*6*).[22]
x (mass %): 5 (*2*), 7 (*3*), 10 (*4*), 12 (*5*).

shown in Fig. 22. The conductivity changes insignificantly, thus indicating thermodynamic stability of this composite. The transfer number of oxygen ions (t_i) increases as the temperature and volume fraction of the liquid phase increase (Fig. 23) and reaches a value of 0.75.

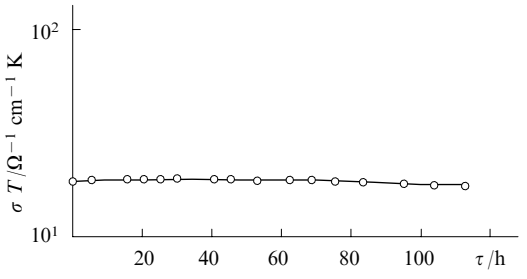


Figure 22. Conductivity-*vs.*-time plot for the $BiVO_4-V_2O_5$ (10 mass %) composite with the liquid-channel grain-boundary structure at 650 °C.[22]

Ion-transport membranes based on $BiVO_4-V_2O_5$ composites with the liquid-channel grain-boundary structure exhibit highly selective oxygen permeation.[20, 22, 210]

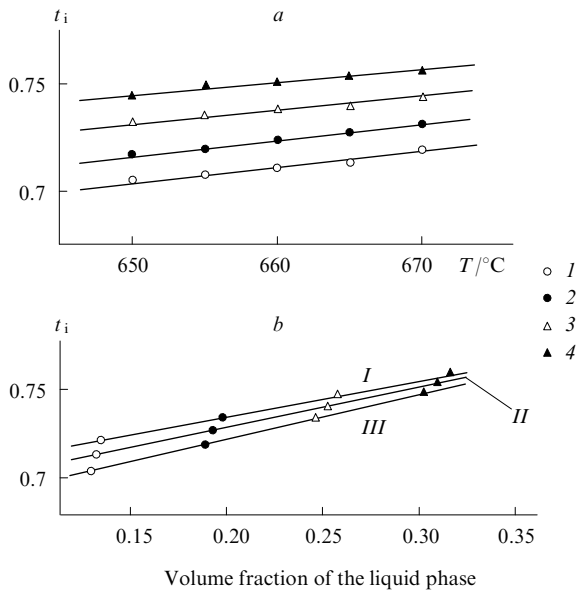


Figure 23. Oxygen ion transfer number (t_i) in the $BiVO_4 - x\,V_2O_5$ composites with the liquid-channel grain-boundary structure plotted *vs.* temperature (*a*) and volume fraction of the liquid phase (*b*).[210]
x (mass %): 5 (*1*), 7 (*2*), 10 (*3*), 12 (*4*); *T*/°C: 670 (*I*), 660 (*II*), 650 (*III*).

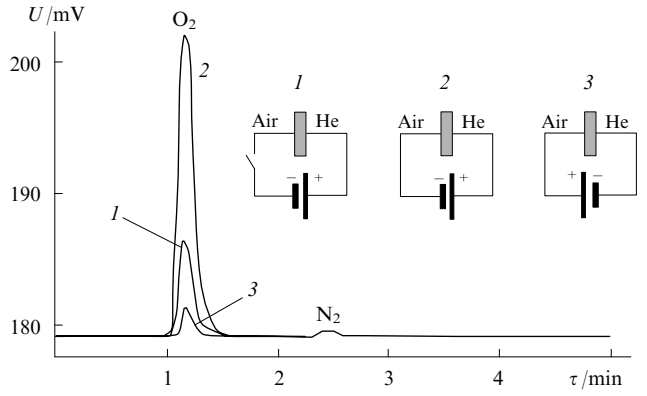


Figure 24. Chromatograms of gas flux through a $BiVO_4 - V_2O_5$ (10 mass %) membrane with the liquid-channel grain-boundary structure at 650 °C.[210]
(*1*) No external electric field; (*2* and *3*) in external electric field of different polarity; *U* is the sensor signal.

Figure 24 shows a chromatogram of a gas penetrated from air through a membrane with the liquid-channel grain-boundary structure under the action of the partial pressure difference between nitrogen and oxygen. The membrane is permeable to oxygen ions and impermeable to nitrogen (weak N_2 peak in Fig. 24 is due to leakage in the manifold). The oxygen permeation is confirmed by the dependence of the oxygen flux on the polarity of applied electric field[210] (Fig. 24). The maximum oxygen concentration in the gas flux was observed when the negative electrode was positioned on the outer surface of the sample (the sample/air interface, see curve *2*). This fact indicates that oxygen ions are transferred through the membrane because the electric field affects only charged particles. The oxygen flux increases with increase in the oxygen partial pressure difference and the temperature (Fig. 25). The dependences of the oxygen flux on the membrane thickness are shown in Fig. 26.

A scheme illustrating oxygen transfer through a $BiVO_4 - V_2O_5$ membrane with the liquid-channel grain-boundary structure is shown in Fig. 27. The process involves the surface oxygen exchange, diffusion of oxygen ions along intergranular liquid channels and electron transfer in the liquid and solid phases (coupled chemical diffusion of ions and electrons).[20, 22, 196–210] The coupled chemical diffusion (and/or surface exchange reactions) is the rate determining step for the overall process.

Consider the diffusion regime of oxygen transfer through the membrane with the liquid-channel grain-boundary structure. In this case, the kinetics is controlled by the coupled chemical diffusion of oxygen ions and electrons. Under the action of the chemical potential gradient, oxygen ions migrate towards regions with low partial pressure of oxygen. Since the oxygen ions are charged, such a migration results in the appearance of an electric field in the membrane, which gives rise to electron transfer through the membrane towards regions with higher partial pressure of oxygen (to maintain electroneutrality). Charged particles (ions) should response to both the chemical and electric potential gradients whose joint action creates the electro-

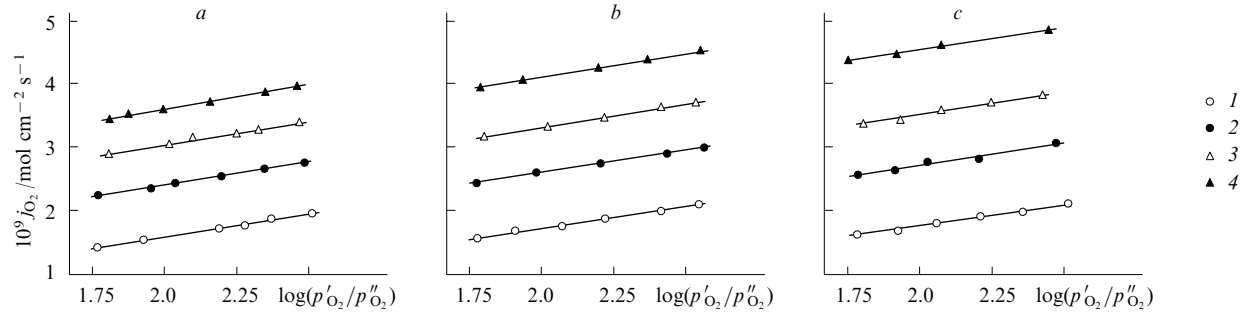


Figure 25. Oxygen fluxes (*j*) through $BiVO_4 - x\,V_2O_5$ membranes (0.2 cm thick) with the liquid-channel grain-boundary structure plotted *vs.* oxygen partial pressure difference at 650 (*a*), 660 (*b*), 670 °C (*c*).[210]
x (mass %): 5 (*1*), 7 (*2*), 10 (*3*), 12 (*4*).

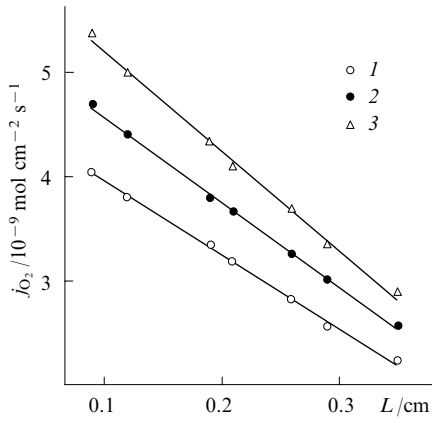


Figure 26. Oxygen fluxes plotted *vs.* thickness (L) of a $BiVO_4-V_2O_5$ (10 mass %) membrane with the liquid-channel grain-boundary structure [$\log(p'_{O_2}/p''_{O_2}) = 2.32$] at 650 (*1*), 660 (*2*) and 670 °C (*3*).[20]

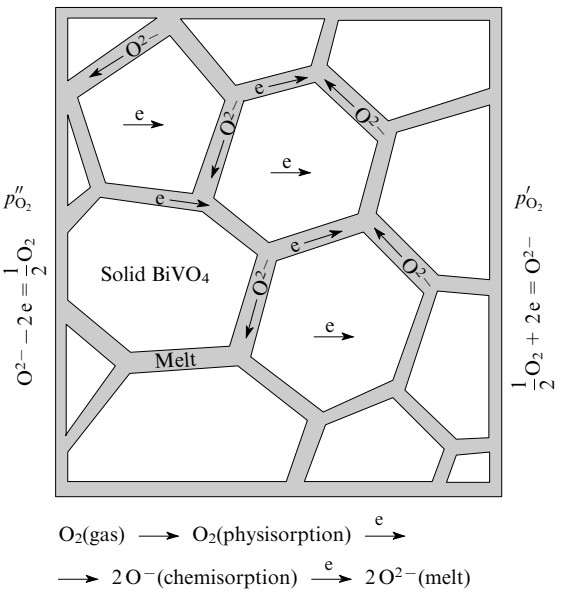


Figure 27. The diagram of oxygen ion and electron transfer in a $BiVO_4-V_2O_5$ membrane with the liquid-channel grain-boundary structure at $p'_{O_2} \gg p''_{O_2}$.[20]

chemical potential gradient that drives ion migration. The oxygen flux through the membrane obeys the Wagner equation

$$j_{O_2} = -\frac{RT}{16\,F^2 L}\int_{\ln p'_{O_2}}^{\ln p''_{O_2}} \sigma_{amb}\, d\ln p_{O_2}, \qquad (35)$$

where F is the Faraday constant and σ_{amb} is the ambipolar conductivity

$$\sigma_{amb} = \frac{\sigma_i \sigma_e}{\sigma_{rmi} + \sigma_e} = t_i(1 - t_i)\sigma, \qquad (36)$$

σ_i, σ_e are the ionic and electronic conductivities, respectively. Taking into account expression (36), the oxygen flow can be written as

$$j_{O_2} = \frac{RT}{16\,F^2 L}\, t_i(1 - t_i)\sigma \ln\frac{p'_{O_2}}{p''_{O_2}}. \qquad (37)$$

This equation is satisfied only if the average value of σ_{amb} is taken for the partial pressure range $p'_{O_2} - p''_{O_2}$.

The specific oxygen flux through the $BiVO_4-V_2O_5$ membrane with the liquid-channel grain-boundary structure for a given difference in the partial pressure of oxygen can be obtained by substituting the experimental values of the conductivity and transfer numbers of oxygen ions (see Figs 21 and 23) into Eqn (37).

According to Eqn (37), the dependence of the oxygen flux on the reciprocal membrane thickness should be linear in the diffusion regime. Figure 28*a* shows the calculated and experimentally observed dependences of the specific oxygen flux on L^{-1}. It is seen that the experimental dependence is nonlinear. Probably, oxygen transfer through the $BiVO_4-V_2O_5$ membranes with the liquid-channel grain-boundary structure proceeds in a mixed diffusion-kinetic regime.

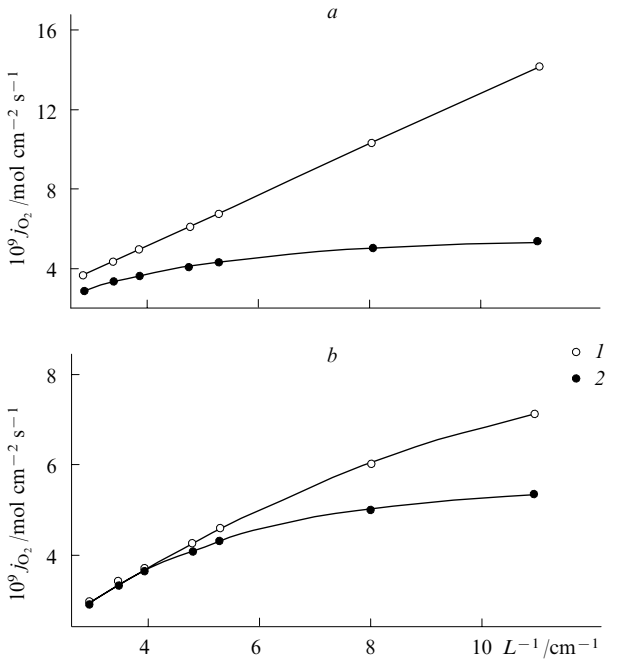


Figure 28. Theoretical (*1*) and experimental (*2*) dependences of oxygen flux on the thickness of $BiVO_4-V_2O_5$ (10 mass %) membrane with the liquid-channel grain-boundary structure [$\log(p'_{O_2}/p''_{O_2}) = 2.32$] at 670 °C.
(*a*) calculated from Eqn (37) (*1*); (*b*) calculated from Eqn (38) (*1*).

Consider this regime of oxygen transfer through a membrane with the liquid-channel grain-boundary structure within the framework of the Burggraaf–Bouwmeester model.[211–213] In this case, the kinetics of oxygen transfer through composites is controlled by both coupled chemical diffusion of ions and electrons and by the surface oxygen exchange reactions. According to the Burggraaf–Bouw-

meester model, the oxygen flux through the membrane is given by

$$j_{O_2} = \frac{RT}{L + 2L_c} \frac{\sigma_{amb}}{16F^2} \ln \frac{p'_{O_2}}{p''_{O_2}}. \quad (38)$$

where L_c is the characteristic thickness of the membrane. At $L \gg L_c$, oxygen transfer proceeds in the diffusion regime; at $L \ll L_c$ it occurs in the kinetic regime

$$L_c = t_e \frac{D_i}{k}, \quad (39)$$

where t_e is the electron transfer number, D_i ($cm^2\ s^{-1}$) is the effective diffusion coefficient of oxygen ions in the membrane with the liquid-channel grain-boundary structure, k ($cm\ s^{-1}$) is the surface oxygen exchange coefficient. In accordance with the Nernst–Einstein equation,

$$D_i = \frac{\sigma_i RT}{c_i z_i^2 F^2}, \quad (40)$$

where c_i is the concentration of oxygen ions (about 10^{-2} mol cm^{-3} for melts, see Ref. 214) and z_i is the charge of the oxygen ion.

The theoretical [calculated by expression (38)] and experimental dependences of the specific oxygen flux on L^{-1} are shown in Fig. 28 *b*. In j_{O_2} calculations, the L_c value was varied to obtain the best fit between the theoretical and experimental curves. A comparison showed that the calculated curve matches the experimental one if the membrane thickness is within 2–4 mm. For such thicknesses, oxygen transfer occurs in the mixed diffusion-kinetic regime. On further reduction of the membrane thickness, the process mainly proceeds in the kinetic regime.

The experimental values of oxygen fluxes and the parameters D_i, σ_{amb} and k calculated using expressions (40), (36) and (39), respectively, as well as the estimated characteristic thicknesses L_c of the membranes based on the $BiVO_4 - x\,V_2O_5$ composites [x = (5, 7, 10, 12) mass %] with the liquid-channel grain-boundary structure are collected in Table 1. As can be seen, the $BiVO_4 - V_2O_5$ (12 mass %) composite exhibits high oxygen permeation and can probably be used as the ion-transport membrane in electrochemical apparatuses for oxygen separation operating at 650–670 °C.

Table 2. Oxygen fluxes through the $BiVO_4 - V_2O_5$ (12 mass %) composite with the liquid-channel grain-boundary structure and through known membrane materials.

Composition	L /cm	T /°C	p'_{O_2} /atm	$p''_{O_2} \times 10^6$ /atm	$j_{O_2} \times 10^9$ (see [a])
$(Bi_2O_3)_{0.75}(Er_2O_3)_{0.25}$	0.11	650	1	1.4	1.9
$(Bi_2O_3)_{0.75}(Er_2O_3)_{0.25} - Ag$	0.13	650	1	2.0	9.7
$(Bi_2O_3)_{0.73}(CaO)_{0.27}$	0.12	650	1	2.2	2.3
$(Bi_2O_3)_{0.73}(CaO)_{0.27} - Ag$	0.08	680	1	2.5	3.0
BICOVOX	0.17	650	1	1.9	1.6
BICOVOX – Au	0.12	650	1	2.0	1.6
$BiVO_4$ – 12 mass % V_2O_5	0.20	650	0.21	1.5×10^3	3.7

Note. The j_{O_2} values were taken from Ref. 210 for the $BiVO_4 - V_2O_5$ (12 mass %) composite and from Ref. 29 for other compounds. [a] In mol $cm^{-2}\ s^{-1}$.

The specific oxygen fluxes through the $BiVO_4 - V_2O_5$ (12 mass %) composite with the liquid-channel grain-boundary structure and through known ion-transport membranes are presented in Table 2. A comparative analysis shows that, with respect to its permeation, this composite ranks second after $(Bi_2O_3)_{0.73}(CaO)_{0.27} - Ag$ and $(Bi_2O_3)_{0.75}(Er_2O_3)_{0.25} - Ag$ cermets. However, the latter are of limited use because of high cost (they contain expensive noble metals). Thus, the $BiVO_4 - V_2O_5$ (12 mass %) composite is more preferable.

2. High-temperature metal corrosion

A priority task in high-temperature materials science is to design novel heat-resistant materials for nuclear and fuel power engineering, space and aircraft industries, *etc*. Practical solution to this task to a great extent depends on the development of theoretical concepts in the field of high-temperature oxidation of metals. In this case, the oxidation rate in the formation of dense oxide layers on metals is controlled by diffusion processes. Namely, it is determined by volume diffusion of reacting ions and by electron transfer through the growing oxide layer. The Wagner model [215] takes account of these processes and gives quantitative relationships between the metal oxidation rate, ion diffusion coefficient and partial pressure of oxygen. The formation of a liquid-channel grain-boundary structure in oxide layers results in strong acceleration of oxidation and catastrophic degradation of the metal.[15–19] Consider the kinetics and

Table 1. Parameters j_{O_2}, D_i, σ_{amb}, k and L_c of $BiVO_4 - x\,V_2O_5$ [x = (5, 7, 10, 12) mass %] composites with the liquid-channel grain-boundary structure.[210]

Composition	T/°C	η	$p''_{O_2} \times 10^3$ /atm	$j_{O_2} \times 10^9$ /mol $cm^{-2}\ s^{-1}$	$D_i \times 10^7$, /$cm^2\ s^{-1}$	$\sigma_{amb} \times 10^3$ /$\Omega^{-1}\ cm^{-1}$	$k \times 10^6$ /cm s^{-1}	L_c/cm
$BiVO_4$ – 5 mass % V_2O_5	650	0.12	5.5	1.9	0.9	1.3	1.3	0.021
	670	0.13	6.1	2.1	1.2	1.5	2.1	0.015
$BiVO_4$ – 7 mass % V_2O_5	650	0.18	8.6	2.6	1.9	2.6	1.3	0.043
	670	0.19	9.6	3.0	2.4	3.1	2.1	0.030
$BiVO_4$ – 10 mass % V_2O_5	650	0.23	1.0	3.2	3.0	3.9	1.3	0.063
	670	0.24	1.2	3.7	3.8	4.6	2.1	0.045
$BiVO_4$ – 12 mass % V_2O_5	650	0.29	1.5	3.7	4.6	5.6	1.3	0.091
	670	0.30	1.8	4.6	5.4	6.3	2.1	0.062

Note. For all compositions, L = 0.2 cm; η is the volume fraction of the liquid phase.

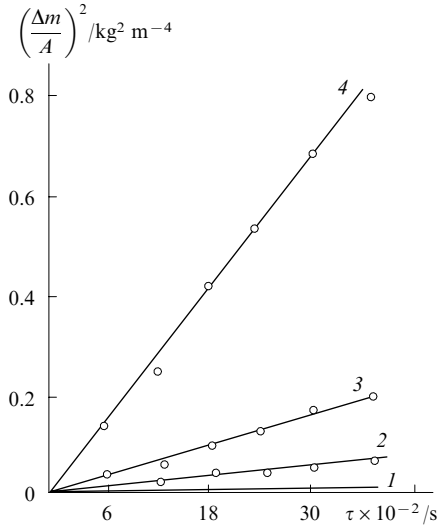


Figure 29. Oxidation kinetics of copper coated with a Bi_2O_3 film at 800 °C.
Film thickness /10^{-5} m: 0 (*1*), 3 (*2*), 6 (*3*), 9 (*4*); $k'' \times 10^5$ /kg² m^{-4} s^{-1}: 0.012 (*1*), 1.6 (*2*), 4.9 (*3*), 21 (*4*); temperature: 800 °C.

mechanism of accelerated metal oxidation using the system $Cu-Bi_2O_3$ as an example; this system best demonstrates the general regularities typical of other systems.[216–219]

Studies of high-temperature oxidation of copper plates ($20 \times 20 \times 0.2-0.5$ mm) coated with a thin Bi_2O_3 layer (30–100 μm) in air showed [12, 15–19] that accelerated copper oxidation occurs at 770 °C. The kinetics of this process at different Bi_2O_3 film thicknesses are shown in Fig. 29. The oxidation of copper is described by a parabolic dependence on time

$$\left(\frac{\Delta m}{A}\right)^2 = k''\tau, \qquad (41)$$

where Δm is the change in the sample mass, A is the copper surface area, k'' is the parabolic oxidation rate constant and τ is time. This dependence indicates a diffusion-controlled process. The k'' value increases with increasing the Bi_2O_3 film thickness and exceeds the parabolic oxidation rate constant of copper by more than three orders of magnitude.

The microstructure of the corrosion product formed during copper oxidation is shown in Fig. 30. The outer (grey) layer mainly consists of Bi_2CuO_4 with small amounts of Bi_2O_3. The inner (light-coloured) layer consists of CuO and small amounts of Cu_2O, Bi_2O_3 and Bi_2CuO_4. The concentrations of Cu_2O and Bi_2O_3 abruptly increase near the copper surface. The location of the oxide layers in the corrosion product indicates that oxidation occurs by oxygen diffusion from air through the oxide layers to copper.

According to the phase diagram of the Bi_2O_3-CuO system (Fig. 31), the threshold temperature of 770 °C for the accelerated copper oxidation coincides with the melting point of δ-$Bi_2O_3-Bi_2CuO_4$ eutectic. Hence, the accelerated oxidation is caused by the formation of the liquid phase in the corrosion product.

Studies [11, 15–19, 99] of the influence of the liquid phase on the transport properties of the oxide layers formed during accelerated oxidation of copper revealed a wetting transition at triple junctions and Bi_2CuO_4 grain boundaries in the presence of eutectic melt and the formation of liquid-channel grain-boundary structure in the Bi_2O_3-CuO and $Bi_2O_3-Bi_2CuO_4$ ceramic composites at 770 °C. Consider this phenomenon using a $Bi_2CuO_4-Bi_2O_3$ (20 mass %) ceramic composite as an example. Figure 32 *a* shows the initial microstructure of this composite. As can be seen, Bi_2O_3 is randomly distributed in the composite. When the sample is heated above 770 °C, the wetting transition at triple junctions and grain boundaries in the presence of eutectic melt and the formation of liquid-channel grain-boundary structure occur (Fig. 32 *b*,*c*). The formation of such a structure significantly affects the transport properties of the oxide layers.[192, 193] Figure 33 demonstrates the dependence of the ionic conductivity with respect to oxygen for the $Bi_2CuO_4-Bi_2O_3$ composites with the liquid-channel grain-boundary structure on the volume fraction of the liquid phase.

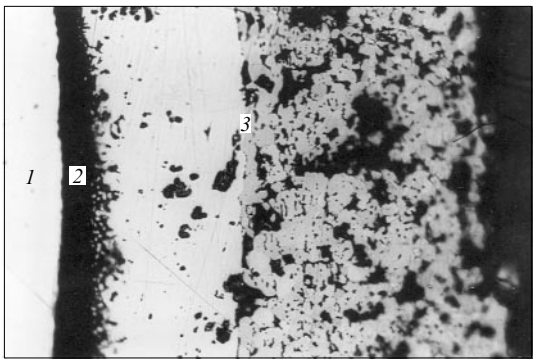


Figure 30. Microstructure of the corrosion product on the copper surface precoated with Bi_2O_3 film and partially oxidized in air at 800 °C.[12]
Copper (*1*); gap formed upon product detachment in the course of cooling (*2*) and product (*3*).

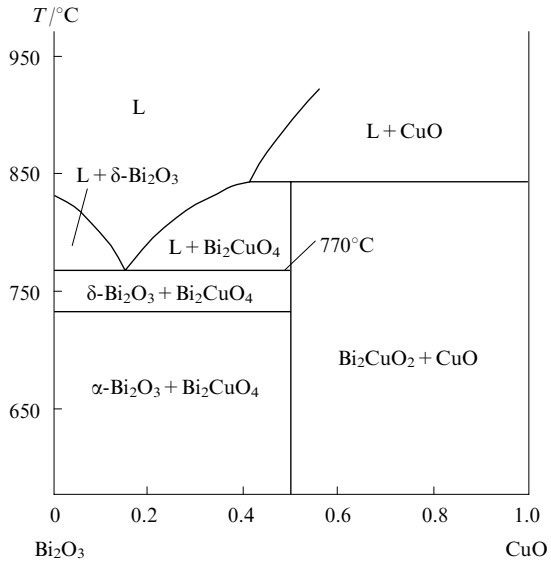


Figure 31. Phase diagram of the system Bi_2O_3-CuO.[220, 221]

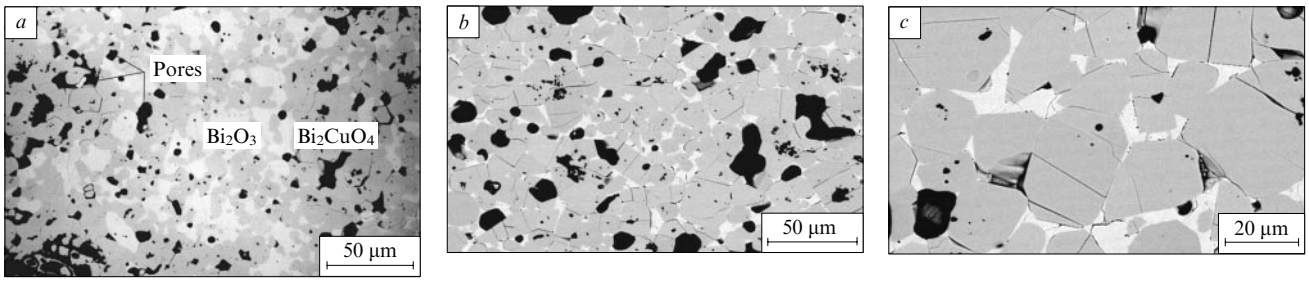


Figure 32. Microstructure of $Bi_2CuO_4-Bi_2O_3$ (20 mass %) ceramic composite. Cooling from 700 °C (*a*); cooling from 780 °C (*b*, *c*).

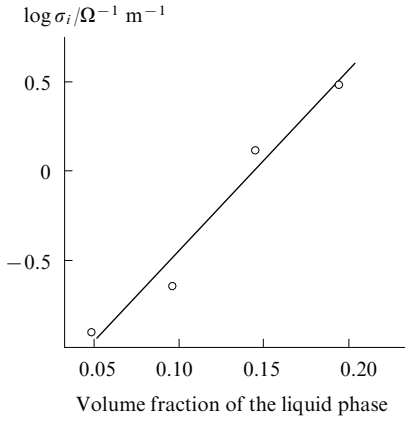


Figure 33. Ionic conductivity with respect to oxygen (σ_i) of $Bi_2CuO_4-x\,Bi_2O_3$ composites [x = (5, 10, 15, 20) mass %] with the liquid-phase grain-boundary structure plotted *vs.* volume fraction of the liquid phase.[18]

Consider the mechanism of accelerated oxidation of copper. Suppose that at instant τ the thickness of the oxide layer on the copper surface is h. Let h be much larger than the distance at which the effect of the spatial charge is significant. A liquid-channel grain-boundary structure forms in the oxide layer. Diffusion of oxygen ions along the liquid intergranular channels limits the rate of copper oxidation. (Solubility of oxygen in the metal is neglected.) Having denoted the concentration of oxygen in the growing oxide by c*, the mass balance equation takes the form:

$$c^*\left(\frac{\mathrm{d}h}{\mathrm{d}\tau}\right)=j_{\mathrm{O}_2}. \tag{42}$$

The oxygen ion flux is given by

$$j_{\mathrm{O}_2}=\frac{RT}{z^2\mathrm{F}^2h}\int\limits_{\ln p''_{\mathrm{O}_2}}^{\ln p'_{\mathrm{O}_2}}\frac{\sigma_\mathrm{i}\sigma_\mathrm{e}}{\sigma_\mathrm{i}+\sigma_\mathrm{e}}\,\mathrm{d}\ln p_{\mathrm{O}_2}, \tag{43}$$

p'_{O_2} and p''_{O_2} are the partial pressures of oxygen at the air/oxide layer and the oxide layer/metal interfaces. At $\sigma_\mathrm{e}\gg\sigma_\mathrm{i}$, Eqn (43) takes the form

$$j_{\mathrm{O}_2}=\frac{RT}{z^2\mathrm{F}^2h}\int\limits_{\ln p''_{\mathrm{O}_2}}^{\ln p'_{\mathrm{O}_2}}\sigma_\mathrm{i}\,\mathrm{d}\ln p_{\mathrm{O}_2}. \tag{44}$$

The parabolic time law for metal oxidation is usually expressed as follows:

$$\frac{\mathrm{d}h}{\mathrm{d}\tau}=\frac{k'}{h}, \tag{45}$$

where k' is the parabolic oxidation rate constant. Using Eqns (42), (44) and (45), k' can be represented as

$$k'=\frac{RT}{z^2\mathrm{F}^2c}\int\limits_{\ln p''_{\mathrm{O}_2}}^{\ln p'_{\mathrm{O}_2}}\sigma_\mathrm{i}\,\mathrm{d}\ln p_{\mathrm{O}_2}. \tag{46}$$

The parabolic oxidation rate constants k' (m^2 s^{-1}) and k'' (kg^2 m^{-4} s^{-1}) are interrelated:

$$k'=\frac{z^2V^2}{2M^2}\,k'', \tag{47}$$

where V is the molar volume of the oxide and M is the molar mass.

$$k''=\frac{2RTM^2}{z^4V^2\mathrm{F}^2c}\int\limits_{\ln p''_{\mathrm{O}_2}}^{\ln p'_{\mathrm{O}_2}}\sigma_\mathrm{i}\,\mathrm{d}\ln p_{\mathrm{O}_2}, \tag{48}$$

or

$$k''=\frac{2RTM^2\sigma_\mathrm{i}}{z^4V^2\mathrm{F}^2c}\,\mathrm{d}\ln\frac{p'_{\mathrm{O}_2}}{p''_{\mathrm{O}_2}}. \tag{49}$$

Equation (49) holds only if the average σ_i value is taken for the oxygen partial pressure range $p'_{\mathrm{O}_2}-p''_{\mathrm{O}_2}$. A comparison of the experimental parabolic oxidation rate constants k'' with the values calculated using expression (49) at $T=10^3$ K, $A^2=6.4\times10^{-3}$ kg^2 mol^{-2}, $V^2=1.5\times10^{-10}$ m^6 mol^{-2}, $c\approx4.0\times10^4$ mol m^{-3}, $p'_{\mathrm{O}_2}=0.21$ atm, $\sigma_\mathrm{i}=0.14-3.6\ \Omega^{-1}$ m^{-1} and $p''_{\mathrm{O}_2}\approx10^{-3}$ atm showed that they are of the same order of magnitude, being equal to $7.5\times10^{-5}-4.0\times10^{-4}$ and $1.6\times10^{-5}-2.1\times10^{-4}$ kg^2 m^{-4} s^{-1}, respectively, which indicates agreement between the theory and experiment.

* * *

Improvement of existing materials and the design of novel systems possessing high mixed conductivity is dictated by the demands of rapidly developing electrochemical power engineering. A possible way to meet these demands is to utilize materials with liquid-channel grain-boundary structures. However, there is a number of unsolved problems on

this way; in particular, the mechanisms of ionic and electronic conductivity in oxide melts,[222] electrokinetic effects,[223] transport properties of interphase boundaries [224] and recrystallization processes are studied insufficiently. Solving these problems will make it possible to advance considerably in understanding of fundamental mechanisms of mass transfer in the liquid-channel grain-boundary structures and to objectively assess prospects for their use in various electrochemical devices.

References

1. P Knauth, H L Tuller *J. Am. Ceram. Soc.* **85** 1654 (2002)
2. P Knauth *J. Electroceram.* **5** 111 (2000)
3. C C Liang *J. Electrochem. Soc.* **120** 1289 (1973)
4. N Sata, K Eberman, K Eberl, J Maier *Nature (London)* **408** 946 (2000)
5. V V Belousov *J. Eur. Ceram. Soc.* **27** 3459 (2007)
6. V V Belousov *Zh. Fiz. Khim.* **81** 521 (2007) [a]
7. J Maier *Solid State Ionics* **157** 327 (2003)
8. J Maier *Solid State Ionics* **175** 7 (2004)
9. J W Cahn *J. Chem. Phys.* **66** 3667 (1977)
10. R H French *J. Am. Ceram. Soc.* **83** 2117 (2000)
11. V V Belousov *J. Mater. Sci.* **40** 2361 (2005)
12. V V Belousov *Oxid. Met.* **42** 511 (1994)
13. V V Belousov *J. Am. Ceram. Soc.* **79** 1703 (1996)
14. V V Belousov *Elektrokhimiya* **31** 1343 (1995) [b]
15. V V Belousov *Russ. Chem. Rev.* **67** 563 (1998) [*Usp. Khim.* **67** 631 (1998)]
16. V V Belousov *Oxid. Met.* **67** 235 (2007)
17. V V Belousov *Russ. J. Phys. Chem., Ser. A* **82** 2243 (2008)
18. V V Belousov *Corros. Sci.* **52** 68 (2010)
19. V V Belousov *Zashch. Met.* **30** 599 (1994) [c]
20. V V Belousov, S V Fedorov, A V Vorobiev *J. Electrochem. Soc.* **158** B601 (2011)
21. RF P. 2400293 (2010); *Byull. Izobret.* (27) (2010)
22. S V Fedorov, V V Belousov, A V Vorobiev *J. Electrochem. Soc.* **155** F241 (2008)
23. I Kul'bakin, V Belousov, S Fedorov, A Vorobiev *Mater. Lett.* **67** 139 (2012)
24. P N Dyer, R E Richards, S L Russek, D M Taylor *Solid State Ionics* **134** 21 (2000)
25. H J M Bouwmeester, A J Burggraaf, in *Fundamentals of Inorganic Membrane Science and Technology* (Eds A J Burggraaf, L Cot) (Amsterdam: Elsevier, 1996) p. 435
26. B A van Hassel *Solid State Ionics* **174** 253 (2004)
27. E W J Römer, U Nigge, T Schulte, H-D Wiemhöfer, H J M Bouwmeester *Solid State Ionics* **140** 97 (2001)
28. L Qiu, T H Lee, L M Liu, Y L Yang, A J Jacobson *Solid State Ionics* **76** 321 (1995)
29. E Capoen, M S Steil, G Nowogrocki, M Malys, C Provano, A Löfberg, E Bordes-Richard, J C Boivin, G Mairesse, R N Vannier *Solid State Ionics* **177** 483 (2006)
30. E Capoen, G Nowogrocki, S J Skinner, J A Kilner, M Malys, J C Bovin, G Mairesse, R N Vannier *Solid State Ionics* **177** 489 (2006)
31. V V Belousov *Pis'ma Zh. Eksp. Teor. Fiz.* **88** 259 (2008) [d]
32. J Sunarso, S Baumann, J M Serra, W A Meulenberg, S Liu, Y S Lin, J C Diniz da Costa *J. Membr. Sci.* **320** 13 (2008)
33. S M Hashim, A R Mohamed, S Bhatia *Adv. Colloid Interface Sci.* **160** 88 (2010)
34. S V Kalinin, R Shao, D A Bonnell *J. Am. Ceram. Soc.* **88** 1077 (2005)
35. V Vitek, A P Sutton, G-J Wang, D Schwartz *Scr. Met.* **17** 183 (1983)
36. D Wolf, J F Lutsko *Z. Kristallogr.* **189** 239 (1989)
37. W T Read, W Shockley *Phys. Rev.* **78** 275 (1950)
38. W Bollmann, in *Crystal Defects and Crystalline Interfaces* (Berlin: Springer, 1970) p. 368
39. H Gleiter *Phys. Status Solidi B* **45** 9 (1971)
40. S Ranganathan *Acta Crystallogr.* **21** 197 (1966)
41. D M Saylor, G S Rohrer *J. Am. Ceram. Soc.* **82** 1529 (1999)
42. P Wynblatt, M Takashima *Interface Sci.* **9** 265 (2001)
43. D M Saylor, G S Rohrer, in *ICOTOM-12. Proceedings of the Twelfth International Conference on Textures of Materials* Vol. 2 (Ottawa: NRC Reserch Press, 1999) p. 1690
44. A D Rollett, C-C Yang, W W Mullins, B L Adams, C T Wu, D Kinderlehrer, S Ta'asan, F Manolache, C Liu, I Livshits, D Mason, A Talukder, S Ozdemir, D Casasent, A Morawiec, D Saylor, G S Rohrer, M Demirel, B El-Dasher, W Yang, in *International Conference on Grain Growth and Recrystallization (Abstracts of Papers), Aachen, 2001* p. 165
45. Ch V Kopetskii, A N Orlov, L K Fionova *Granitsy Zeren v Chistykh Materialakh* (Grain Boundary in Pure Materials) (Moscow: Nauka, 1987)
46. V L Pokrovskii, A L Talapov *Zh. Eksp. Teor. Fiz.* **78** 269 (1980) [e]
47. A A Zisman, V V Rybin *Poverkhnost. Fiz., Khim., Mekhan.* **7** 87 (1982)
48. A P Sutton, R W Balluffi *Interfaces in Crystalline Materials* (Oxford: Clarendon Press, 1995)
49. B S Bokshtein, Ch V Kopetskii, L S Shvindlerman *Termodinamika i Kinetika Granits Zeren v Metallakh* (Thermodynamics and Kinetics of Grain Boundaries in Metals) (Moscow: Metallurgiya, 1986)
50. E I Rabkin, L S Shvindlerman, B B Straumal *Int. J. Mod. Phys. B* **5** 2989 (1991)
51. R W Balluffi, R Maurer *Scr. Met.* **22** 709 (1988)
52. B B Straumal *Fazovye Perekhody na Granitsakh Zeren* (Phase Transitions at Grain Boundaries) (Moscow: Nauka, 2003)
53. A L Petelin, Doctoral Thesis in Physical and Mathematical Sciences, National University of Science and Technology, Moscow, 2007
54. P-G de Gennes *Usp. Fiz. Nauk* **151** 619 (1987) [f]
55. D R Clarke *Ultramicroscopy* **4** 33 (1979)
56. M R Moldover, J W Cahn *Science* **207** 1073 (1980)
57. P Wynblatt, D Chatain *Mat. Sci. Eng. A* **495** 119 (2008)
58. H Kellay, D Bonn, J Meunier *Phys. Rev. Lett.* **71** 2607 (1993)
59. J W Schmidt, M R Moldover *J. Chem. Phys.* **79** 379 (1983)
60. K Nord-Varhaug *J. Am. Ceram. Soc.* **79** 1147 (1996)
61. M Fujimoto, W D Kingery *J. Am. Ceram. Soc.* **68** 169 (1985)
62. W D Kingery, J B Van der Sande, T Mitamura *J. Am. Ceram. Soc.* **62** 221 (1979)
63. M Matsuoka *Jpn. J. Appl. Phys.* **10** 736 (1971)
64. J P Gambino, W D Kingery, G E Pike, L M Levinson, H R Philipp *J. Am. Ceram. Soc.* **72** 642 (1989)
65. E Olsson, G L Dunlop *J. Appl. Phys.* **66** 4317 (1989)
66. V V Belousov *Neorg. Mater.* **39** 94 (2003) [g]
67. V V Belousov *Kolloid. Zh.* **66** 149 (2004) [h]
68. J W Gibbs, in *The Scientific Paper of J Willard Gibbs: Thermodynamics* (Oxford: Bow Press, 1993) p. 462
69. H J Kleebe, M K Cinibulk, R M Cannon, M Rühle *J. Am. Ceram. Soc.* **76** 1969 (1993)
70. H J Kleebe, M J Hoffman, M Ruhle *Z. Metallkd.* **83** 610 (1992)
71. G M Safronov, V N Batog, T V Stepanyuk, P M Fedorov *Zh. Neorg. Khim.* **16** 460 (1971) [i]
72. D E Newbury, D B Williams *Acta Mater.* **48** 323 (2000)
73. J Luo, Y-M Chiang *Acta Mater.* **48** 4501 (2000)
74. D L Callahan, G Thomas *J. Am. Ceram. Soc.* **73** 2167 (1990)
75. K M Knowles, S Turan *Ultramicroscopy* **83** 245 (2000)
76. P E D Morgan, D R Clarke, C M Jantzen, A B Barker *J. Am. Ceram. Soc.* **64** 249 (1981)
77. M M R Boutz, C S Chen, L Winnubst, A J Burggraaf *J. Am. Ceram. Soc.* **77** 2632 (1994)

78. A Subramaniam, C T Koch, R M Cannon, M Rühle *Mater. Sci. Eng., A* 422 (2006)
79. F Ernst, O Kienzle, M Rühle *J. Eur. Ceram. Soc.* **19** 665 (1999)
80. D R Clarke *J. Am. Ceram. Soc.* **70** 15 (1987)
81. B Widom *J. Chem. Phys.* **68** 3878 (1978)
82. B Widom *Phase Transitions and Critical Phenomena* (New York: Academic Press, 1972)
83. P-G de Gennes *J. Phys. Lett.* **42** 377 (1981)
84. A W Adamson, A P Gast *Physical Chemistry of Surfaces* (New York: Wiley, 1997)
85. D Tabor, R H S Winterton *Proc. R. Soc. London, Ser. A* **312** 435 (1969)
86. J N Israelachvili, in *Intermolecular and Surface Forces* (Orlando: Academic Press, 1991) p. 480
87. R G Horn, J N Israelachvili *Chem. Phys. Lett.* **71** 192 (1980)
88. R M Pashley, J N Israelachvili *J. Colloid Interface Sci.* **101** 511 (1984)
89. D R Clarke *J. Phys.* **46** 51 (1985)
90. B V Derjaguin, N V Churaev, V M Muller *Poverkhnostnye Sily* (Surface Forces) (Moscow: Nauka, 1985)
91. H C Hamaker *Physica* **4** 1058 (1937)
92. I E Dzyaloshinskii, E M Lifshits, L P Pitaevskii *Usp. Fiz. Nauk* **73** 381 (1961) [f]
93. J W Cahn, J E Hillard *J. Chem. Phys.* **28** 258 (1958)
94. V L Ginzburg, L D Landau *Zh. Eksp. Teor. Fiz.* **20** 1064 (1950) [e]
95. H Wang, Y-M Chiang *J. Am. Ceram. Soc.* **81** 89 (1998)
96. Y-M Chiang, H Wang, J-R Lee *J. Microsc.* **191** 275 (1998)
97. J Luo, H Wang, Y-M Chiang *J. Am. Ceram. Soc.* **82** 916 (1999)
98. R Brydson, S-C Chen , F L Riley, S J Milne, X Pan, M Rühle *J. Am. Ceram. Soc.* **81** 369 (1998)
99. V V Belousov *J. Am. Ceram. Soc.* **82** 1342 (1999)
100. V I Odelevskii *Zh. Tekh. Fiz.* **21** 678 (1951) [j]
101. W W Mullins *J. Appl. Phys.* **30** 77 (1959)
102. E E Glickman, M Nathan *J. Appl. Phys.* **85** 3185 (1999)
103. W M Robertson *Trans. Met. Soc.* **233** 1232 (1965)
104. B S Bokstein, L M Klinger, I V Apikhtina *Mater. Sci. Eng., A* **203** 373 (1995)
105. V E Fradkov *Scr. Metall. Mater.* **30** 1599 (1994)
106. P A Rebinder, E D Shchukin, in *P A Rebinder. Izbrannye Trudy. Fiziko-khimicheskaya Mekhanika* (P A Rebinder. Selected Works. Physochemical Mechanics) (Moscow: Nauka, 1979) Vol. 2, p. 203
107. V V Belousov *J. Supercond.* **15** 207 (2002)
108. E Rabkin, I Snapiro *Acta Mater.* **48** 4463 (2000)
109. C Kittel *Introduction to Solid State Physics* (New York: Wiley, 1975)
110. V V Belousov, V N Konev, A K Roslik *Sverkhprovodimost: Fiz., Khim., Tekh.* **3** 1895 (1990)
111. N Setter, R Waser *Acta Mater.* **48** 151 (2000)
112. B S Bokshtein, A B Yaroslavtsev *Diffuziya Atomov i Ionov v Tverdykh Telakh* (Diffusion of Atoms and Ions in Solids) [Moscow: National University of Science and Technology (MISIS), Moscow, 2005]
113. S F Pal'guev *Zh. Prikl. Khim.* **73** 1745 (2000) [k]
114. D Kuscer, M Hrovat, J Holc, S Bernik, D Kolar *Mat. Res. Bull.* **35** 2525 (2000)
115. J Mizusaki, Y Yonemura, H Kamata, K Ohyama, N Mori, H Takai, H Tagawa, M Dokiya, K Naraya, T Sasamoto, H Inaba, T Hashimoto *Solid State Ionics* **132** 167 (2000)
116. Y Takeda, S Nakai, T Kojima, R Kanno, N Imanishi, G Q Shen, O Yamamoto, M Mori, C Asakawa, T Abe *Mat. Res. Bull.* **26** 153 (1991)
117. J H Kuo, H U Anderson, D M Sparlin *J. Solid State Chem.* **87** 55 (1990)
118. J Y Yi, G M Choi *Solid State Ionics* **148** 557 (2002)
119. N Gunasekaran, N Bakshi, C B Alcock, J J Carberry *Solid State Ionic* **83** 145 (1996)
120. Y Ji, J A Kilner, M F Carolan *Solid State Ionics* **176** 937 (2005)
121. H Fukunaga, M Ihara, K Sakaki, K Yamada *Solid State Ionics* **86–88** 1179 (1996)
122. H Ullmann, N Trofimenko, F Tietz, D Stöver, A Ahmad-Khanlou *Solid State Ionics* **138** 79 (2000)
123. M Al Daroukh, V V Vashook, H Ullmann, F Tietz, I Arual Raj *Solid State Ionics* **158** 141 (2003)
124. L W Tai, M M Nasrallah, H U Anderson, D M Sparlin, S R Sehlin *Solid State Ionics* **76** 259 (1995)
125. A Petric, P Huang, F Tietz *Solid State Ionics* **135** 719 (2000)
126. S-H Byeon, K Park, M Itoh *J. Solid State Chem.* **121** 430 (1996)
127. Y Teraoka, H M Zhang, K Okamoto, N Yamazoe *Mat. Res. Bull.* **23** 51 (1988)
128. A I Rusanov *Solid State Ionics* **75** 275 (1995)
129. Y Teraoka, T Nobunaga, K Okamoto, N Miura, N Yamazoe *Solid State Ionics* **48** 207 (1991)
130. C S Tedmon Jr, H S Spacil, S P Mitoff *J. Electrochem. Soc.* **116** 1170 (1969)
131. S Kuharuangrong *Ceram. Int.* **30** 273 (2004)
132. A Poirson, P Decorse, G Caboche, L C Dufour *Solid State Ionics* **99** 287 (1997)
133. V V Kharton, A V Kovalevsky, A P Viskup, A L Shaula, F M Figueiredo, E N Naumovich, F M B Marques *Solid State Ionics* **160** 247 (2003)
134. V N Tikhonovich, V V Kharton, E N Naumovich, A A Savitsky *Solid State Ionics* **106** 197 (1998)
135. V V Kharton, A A Yaremchenko, M V Patrakeev, E N Naumovich, F M B Marques *J. Eur. Ceram. Soc.* **23** 1417 (2003)
136. A V Kovalevsky, V V Kharton, V N Tikhonovich, E N Naumovich, A A Tonoyan, O P Reut, L S Boginsky *Mater. Sci. Eng., B* **52** 105 (1998)
137. H Taimatsu, K Wada, H Kaneko, H Yamamura *J. Am. Ceram. Soc.* **75** 401 (1992)
138. V V Kharton, A P Viskup, I P Marozau, E N Naumovich *Mat. Lett.* **57** 3017 (2003)
139. H J M Bouwmeester, A J Burggraaf, in *The CRC Handbook of Solid State Electrochemistry* (Eds P J Gellings, H J M Bouwmeester) (Boca Raton, FL: CRC Press, 1997) p. 481
140. V V Kharton, A A Yaremchenko, E N Naumovich *J. Solid State Electrochem.* **3** 303 (1999)
141. Y Teraoka, H M Zhang, S Furukawa, N Yamazoe *Chem. Lett.* **14** 1743 (1985)
142. U Balachandran, J T Dusek, S M Sweeney, R B Poeppel, R L Mieville, P S Maiya, M S Kleefisch, S Pei, T P Kobylinski, C A Udovich, A C Bose *Am. Ceram. Soc. Bull.* **74** 71 (1995)
143. S Pei, M S Kleefisch, T P Kobylinski, J Faber, C A Udovich, V Zhang-McCoy, B Dabrowski, U Balachandran, R L Mieville, R B Poeppel *Catal. Lett.* **30** 201 (1995)
144. J M Ralph, C Rossignol, R Kumar *J. Electrochem. Soc.* **150** A1518 (2003)
145. H C Yu, K Z Fung *Mater. Res. Bull.* **38** 231 (2003)
146. D P Fagg, V V Kharton, J R Frade, A A L Ferreira *Solid State Ionics* **156** 45 (2003)
147. Z Gong, X Yin, L Hong *Solid State Ionics* **180** 1471 (2009)
148. K Zhang, R Ran, L Ge, Z Shao, W Jin, N Xu *J. Alloys Compd.* **474** 477 (2009)
149. P Zeng, Z Chen, W Zhou, H Gu, Z Shao, S Liu *J. Membr. Sci.* **291** 148 (2007)
150. H Wang, C Tablet, A Feldhoff, J Caro *J. Membr. Sci.* **262** 20 (2005)

151. T Ishihara, H Matsuda, Y Takita *J. Am. Chem. Soc.* **116** 3801 (1994)
152. M Ranlov, M Mogensen, F W Poulsen, in *Proceedings of the 14th Riso International Symposium on Materials Science*. (Eds F W Poulsen, J J Bentzen T Jakobsen, E Skou, M J L Ostergard) (Roskilde, Denmark: Riso National Laboratory, 1993) p. 389
153. N J Long, F Lecarpentier, H L Tuller *J. Electroceram.* **3** 399 (1999)
154. J C Boivin, G Mairesse *Chem. Mater.* **10** 2870 (1998)
155. R K B Gover, P R Slater *Annu. Rep. Prog. Chem., Sect. A: Inorg. Chem.* **100** 525 (2004)
156. E V Tsipis, V V Kharton, N P Vyshatko, A L Shaula, J R Frade *J. Solid State Chem.* **176** 47 (2003)
157. B Aurivillius *Ark. Kemi.* **1** 463 (1949)
158. A D Rae, J G Thompson, R L Withers *Acta Crystallogr., Sect. B* **48** 418 (1992)
159. B Frit, J P Mercurio *J. Alloys Compd.* **188** 27 (1992)
160. E C Subbarao *J. Phys. Chem. Solids* **23** 665 (1962)
161. M C Steil, F Ratajczak, E Capoen, C Piravano, R N Vannier, G Mairesse *Solid State Ionics* **176** 2305 (2005)
162. J C Boivin, C Pirovano, G Nowogrocki, G Mairesse, P Labrune, G Lagrange *Solid State Ionics* **113–115** 639 (1998)
163. J Sunarso, S Liu, Y S Lin, J C Diniz da Costa *J. Member. Sci.* **344** 281 (2009)
164. K R Kendall, C Navas, J K Thomas, H C zur Loye *Chem. Mater.* **8** 642 (1996)
165. A-Q Pham, I Yazdi, A J Jacobson *J. Electrochem. Soc.* **142** 1559 (1995)
166. A-Q Pham, M Puri, J F DiCarlo, A J Jacobson *Solid State Ionics* **72** 309 (1994)
167. J B Goodenough, J E Ruiz-Diaz, Y S Zhen *Solid State Ionics* **44** 21 (1990)
168. V Sharma, A K Shukla, J Gopalakrishnan *J. Mater. Chem.* **4** 703 (1994)
169. R N Vannier, G Nowogrocki, G J Mairesse *J. Mater. Chem.* **5** 361 (1995)
170. J K Thomas, M E Anderson, W E Krause, H C zur Loye, in *Materials Research Society Symposium Proceedings: Solid State Ionics* Vol. 293 (Eds G-A Nazri, J-M Tarascon, M Armand) (Boston: MRS, 1992) p. 295
171. J K Thomas, K R Kendall, H C zur Loye *Solid State Ionics* **70–71** 225 (1994)
172. K R Kendall, J K Thomas, H C zur Loye *Chem. Mater.* **7** 50 (1995)
173. K R Kendall, C Navas, H C zur Loye, in *Materials Research Society Symposium Proceedings: Solid State Ionics* Vol. 369 (Eds G-A Nazri, J-M Tarascon, M Armand) (Boston: MRS, 1995) p. 355
174. F Abraham, M F Debruille-Gresse, G Mairesse, G Nowogrocki *Solid Slate Ionics* **28–30** 529 (1988)
175. G Mairesse, in *Fast Ion Transport In Solids* (Ed. B Scrosati) (New York: Kluweri Academic, 1993) p. 271
176. K R Kendall, J K Thomas, H C zur Loye *Solid State Ionics* **70–71** 221 (1994)
177. J R Dygas, F Krok, W Bogusz, P Kurek, K Reiselhuber, M W Breiter *Solid State Ionics* **70–71** 239 (1994)
178. J B Goodenough, A Manthiram, P Paranthaman, Y S Zhen *Solid State Ionics* **52** 105 (1992)
179. T Iharada, A Hammouche, J Fouletier, M Kleitz, J C Boivin, G Mairesse *Solid State Ionics* **48** 257 (1991)
180. O Joubert, A Jouanneaux, M Ganne, R N Vannier, G Mairesse *Solid State Ionics* **73** 309 (1994)
181. E Pernot, M Anne, M Bacmann, P Strobel, J Fouletier, R N Vannier, G Mairesse, F Abraham, G Nowogrocki *Solid Slate Ionics* **70–71** 259 (1994)
182. R N Vannier, G Mairesse, F Abraham, G Nowogrocki *J. Solid State Chem.* **103** 441 (1993)
183. C K Lee, M P Tan, A R West *J. Mater. Chem.* **4** 525 (1994)
184. J B Goodenough, A Manthiram, M Paranthaman, Y S Zhen *Mater. Sci. Eng., B* **12** 357 (1992)
185. A Cherrak, R Hubaut, Y Barbaux, G Mairesse *Catal. Lett.* **15** 377 (1992)
186. A W Sleight, in *Advanced Materials in Catalysis* (Eds J J Burton, R L Garten) (New York: Academic Press, 1977) p. 181
187. R Bredesen *Seminar on the Ecological Applications of Innovative Membrane Technology in the Chemical Industry* (Cetraro, Italy: United Nations Economic Commission for Europe, 1996)
188. J E ten Elshof, N Q Nguyen, M W den Otter, H J M Bouwmeester *J. Electrochem. Soc.* **144** 4361 (1997)
189. A Llfberg, S Boujmiai, E Capoen, M C Steil, C Pirovano, R N Vannier, G Mairesse, E Bordes-Richard *Catal. Today* **91–92** 79 (2004)
190. T J Mazanec *Solid State Ionics* **70–71** 11 (1994)
191. K Huang, M Schroeder, J B Goodenough *Electrochem. Solid State Lett.* **2** 375 (1999)
192. N V Lyskov, Yu G Metlin, V V Belousov, Yu D Tretyakov *Dokl. Akad. Nauk* **392** 63 (2003) [l]
193. N V Lyskov, Yu G Metlin, V V Belousov, Yu D Tretyakov *Solid State Ionics* **166** 207 (2004)
194. V M Skorikov, Yu F Kargin, in *Issledovaniya po Neorganicheskoi Khimii i Khimicheskoi Tekhnologii* (Investigations on Inorganic Chemistry and Chemical Engineering) (Moscow: Nauka, 1988) p. 261
195. R-J Xie, M Mitomo, G-D Zhan *Acta Mater.* **48** 2049 (2000)
196. I C Vinke, J Diepgrond, B A Boukamp, K J de Vries, A J Burggraaf *Solid State Ionics* **57** 83 (1992)
197. V I Musikhin, E A Pastukhov, N A Vatolin, B M Lepinskikh *Neorg. Mater.* **7** 99 (1971) [g]
198. T Allersma, R Hakin, T N Kennedy, J D Mackenzie *J. Chem. Phys.* **46** 154 (1967)
199. D S Volzhenskii, M V Pashkovskii *Fiz. Tv. Tela* **11** 950 (1969) [m]
200. E F Milan *J. Phys. Chem.* **33** 498 (1929)
201. E N Pastukhov, O A Esin, N A Vatolin *Izv. Akad. Nauk SSSR, Neorg. Mater.* **4** 1960 (1968) [g]
202. D A Pantony, K I Vasu *J. Inorg. Nucl. Chem.* **30** 433 (1968)
203. T B Patrina, V A Ioffe *Fiz. Tv. Tela* **6** 2581 (1965) [m]
204. A I Manakov, O A Esin, B M Lepinskikh *Zh. Fiz. Khim.* **36** 1481 (1962) [a]
205. A I Manakov, O A Esin, B M Lepinskikh *Zh. Neorg. Khim.* **7** 1149 (1962) [i]
206. V P Elyutin, Yu A Pavlov, V I Shulepov, T G Myakisheva *Zh. Fiz. Khim.* **36** 813 (1962) [a]
207. V A Yurkov *Zh. Eksp. Teor. Fiz.* **22** 223 (1952) [e]
208. O A Esin, V L Zyazev *Zh. Neorg. Khim.* **2** 1998 (1957) [i]
209. T S Zolyan, A R Regel' *Fiz. Tv. Tela* **6** 1520 (1964) [m]
210. S V Fedorov, Candidate Thesis in Chemical Sciences, Institute of Metallurgy and Materials, Russian Academy of Sciences, Moscow, 2010
211. P J Gellings, H J M Bouwmeester *Catal. Today* **12** 1 (1992)
212. H J M Bouwmeester, H Kruidhof, A J Burggraaf *Solid State Ionics* **72** 185 (1994)
213. C H Chen, H J M Bouwmeester, R H E van Doorn, H Kruidhof, A J Burggraaf *Solid State Ionics* **98** 7 (1997)
214. V S Bagotskii *Osnovy Elektrokhimii* (Foundations of Electrochemistry) (Moscow: Khimiya, 1988)
215. N Birks, G H Meier, F S Pettit *Introduction to the High-Temperature Oxidation of Metals* (2nd Ed.) (Cambridge: Cambridge University Press, 2006)
216. R A Rapp *Corros. Sci.* **44** 209 (2002)
217. R A Rapp *Pure Appl. Chem.* **62** 113 (1990)
218. H Singh, D Puri, S Prakash *Rev. Adv. Mater. Sci.* **16** 27 (2007)
219. T S Sidhu, S Prakash, R D Agrawal *Curr. Sci.* **90** 41 (2006)

220. B Haltstedt, D Risold, L J Gauckler *J. Am. Ceram. Soc.* **79** 353 (1996)
221. M P Kulakov, D Ya Lenchinenko *Thermochim. Acta* **188** 129 (1991)
222. V M Denisov, N V Belousova, S A Istomin, S G Bakhvalov *Stroenie i Svoistva Rasplavlennykh Oksidov* (Structure and Properties of Oxide Melts) (Ekaterinburg: Ural Branch of the Russian Academy of Sciences, 1999)
223. A V Delgado, F Gonzalez-Caballero, R J Hunter, L K Koopal, J Lyklema *Pure Appl. Chem.* **77** 1753 (2005)
224. A A Klimashin, V V Belousov *Elektrokhimiya* **45** 606 (2009) [b]

[a] — *Russ. J. Phys. Chem., Ser. A (Engl. Transl.)*
[b] — *Russ. J. Electrochem. (Engl. Transl.)*
[c] — *Prot. Met. (Engl. Transl.)*
[d] — *J. Exp. Theor. Phys. Lett. (Engl. Transl.)*
[e] — *J. Exp. Theor. Phys. (Engl. Transl.)*
[f] — *Physics-Uspekhi (Engl. Transl.)*
[g] — *Inorg. Mater. (Engl. Transl.)*
[h] — *Colloid. J. (Engl. Transl.)*
[i] — *Russ. J. Inorg. Chem. (Engl. Transl.)*
[j] — *J. Tech. Phys. (Engl. Transl.)*
[k] — *Russ. J. Appl. Chem. (Engl. Transl.)*
[l] — *Dokl. Chem. (Engl. Transl.)*
[m] — *Phys. Solid. State (Engl. Transl.)*